

## RESEARCH ARTICLE

# TRPM2 causes sensitization to oxidative stress but attenuates high-temperature injury in the sea anemone *Nematostella vectensis*

Wiebke Ehrlich<sup>1</sup>, James M. Gahan<sup>2</sup>, Fabian Rentzsch<sup>2</sup> and Frank J. P. Kühn<sup>1,\*</sup>

## ABSTRACT

In humans, the cation channel TRPM2 (HsTRPM2) has been intensively studied because it is involved in oxidative stress-mediated apoptosis and also contributes to temperature regulation. The gating mechanism of TRPM2 is quite complex, with a C-terminally localized enzyme domain playing a crucial role. The analysis of orthologues of TRPM2, in particular from the distantly related marine invertebrate *Nematostella vectensis* (NvTRPM2), revealed that during evolution, the functional role of the endogenous enzyme domain of TRPM2 has undergone fundamental changes. In this study, we investigated whether these evolutionary differences also apply to the physiological functions of TRPM2. For this purpose, we generated a TRPM2 loss-of-function mutation in *N. vectensis* and compared the phenotypes of wild-type and mutant animals after exposure to either oxidative stress or high temperature. Our results show that under standard culture conditions, mutant animals are indistinguishable from wild-type animals in terms of morphology and development. However, exposure of the two experimental groups to different stressors revealed that TRPM2 causes sensitization to oxidative stress but attenuates high-temperature injury in *N. vectensis*. Therefore, NvTRPM2 plays opposite roles in the cellular response to these two different stressors. These findings reveal a similar physiological spectrum of activity of TRPM2 in humans and *N. vectensis* and open up the possibility of establishing *N. vectensis* as a model organism for the physiological function of TRPM2.

**KEY WORDS:** NUDT9, *Nematostella vectensis*, TRPM channels, Environmental stress

## INTRODUCTION

The starlet sea anemone *Nematostella vectensis* has become a prominent model system for genomic and developmental studies (e.g. Layden et al., 2016; Darling et al., 2005). This is mainly due to the fact that, despite the long evolutionary distance, vertebrates and sea anemones retain a striking degree of similarity in gene repertoire and intron/exon structure (Technau et al., 2005; Sullivan et al., 2006; Putnam et al., 2007). Furthermore, these two metazoan groups share many signalling pathways that regulate, for example, development (Technau et al., 2005) and innate immunity (Miller et al., 2007). The natural habitat of *N. vectensis* is shallow and

brackish water zones of the Atlantic and Pacific coast of North America and of the south and east coast of England (Sheader et al., 1997). The environmental conditions in these habitats are highly variable, exposing *N. vectensis* to strong environmental stressors, including changes in temperature, salinity, ultraviolet radiation and levels of reactive oxygen species (Hand and Uhlinger, 1992; Sheader et al., 1997). This is especially true for the contemporary degradation of these habitats as a result of anthropogenic impacts (Harter and Matthews, 2005). It is therefore tempting to also consider *N. vectensis* as a marine invertebrate model system for the response of multicellular organisms to environmental stress (Reitzel et al., 2008; Elran et al., 2014; Tarrant et al., 2014).

The physiological tolerance of an organism is determined by its repertoire of stress response genes. Comparative genetic studies on diverse organisms have revealed that many components of the stress response network are conserved between bilaterians and *N. vectensis*, among them genes involved in the responses to oxidative stress (Reitzel et al., 2008). In humans, the cellular responses induced by oxidative stress have been intensively studied, as they often represent the starting point for numerous pathophysiological processes (e.g. Malko and Jiang, 2020). This specifically includes cellular apoptosis triggered by oxidative stress, which is mediated by the nicotinamide adenine dinucleotide (NAD<sup>+</sup>) metabolite adenosine diphosphate ribose (ADPR; Fonfria et al., 2004; Perraud et al., 2005). It has been shown that in human cells, oxidative stress induces intracellular pathways leading to poly-ADP-ribosylation of DNA and various nuclear proteins. This process is catalysed by the enzyme poly-ADPR polymerase type 1 (PARP-1). Subsequently, poly-ADPR-glycohydrolase (PARG) degrades the poly-ADPR chains to monomeric ADPR (e.g. reviewed in Pascal and Ellenberger, 2015). The resulting increase in the cytosolic ADPR concentration in turn leads to the direct activation of the ADPR-dependent transient receptor potential melastatin type 2 (TRPM2) channel (Perraud et al., 2001, 2005). The binding of ADPR to this non-selective plasma membrane cation channel causes a massive influx of calcium through the channel pore, which in most cases leads to cell death. This indirect activation of HsTRPM2 by oxidative stress can be experimentally simulated by extracellular application of H<sub>2</sub>O<sub>2</sub> (Hara et al., 2002).

A unique feature of TRPM2 is the presence of a C-terminal domain, which is homologous to the human ADPR diphosphatase NUDT9 (Perraud et al., 2001). Initially it was postulated that this domain plays a crucial role in the ADPR-dependent activation of TRPM2 (reviewed in Kühn, 2020). In this regard, however, a paradigm shift recently occurred, as comparative *in vitro* analyses of TRPM2 orthologues, in particular that of *N. vectensis* (NvTRPM2), revealed that the activation of TRPM2 by ADPR also works without the NUDT9 homology (NUDT9H) domain (Kühn et al., 2016; 2017). Moreover, an additional ADPR binding pocket in the

<sup>1</sup>Institute of Physiology, Medical Faculty, University Hospital Aachen, 52074 Aachen, Germany. <sup>2</sup>Sars International Centre for Marine Molecular Biology, University of Bergen, 5008 Bergen, Norway.

\*Author for correspondence (fkuehn@ukaachen.de)

 F.J.P.K., 0000-0003-2514-6287

N-terminal part of TRPM2 has recently been confirmed by cryogenic electron microscopy (Huang et al., 2018, 2019). In the human TRPM2 orthologue, the NUDT9H domain has no enzymatic activity but is indispensable for pore opening (Perraud et al., 2001, 2003; Kühn et al., 2016; Iordanov et al., 2016), whereas in NvTRPM2, NUDT9H has full ADPRase activity but does not affect channel function (Kühn et al., 2016; Iordanov et al., 2019).

Besides its prominent role in oxidative stress mediated apoptosis, in mammals TRPM2 is involved in numerous physiological processes such as immune cell activation (Yamamoto et al., 2008), insulin secretion (Uchida et al., 2011) and innate immunity (Knowles et al., 2013). In humans, TRPM2 was also shown to regulate core body temperature (Tan and McNaughton, 2016; Song et al., 2016). Interestingly, there is experimental evidence that oxidative stress ( $H_2O_2$ ) sensitizes mouse TRPM2 to higher temperatures (Tan and McNaughton, 2016). The interplay of oxidative stress and increased temperature is also of great relevance for the ecology of marine invertebrates. This is particularly true for coral bleaching, which is closely associated with oxidative stress and higher temperatures (e.g. Downs et al., 2002; Dias et al., 2019). In this regard, TRPM2 would represent a promising target to investigate the underlying molecular mechanism in more detail.

Investigations of cellular factors dealing with oxidative stress have been performed in diverse cnidarians, among them *N. vectensis*. In one study, several antioxidant enzymes of the superoxide dismutase family could be identified in *N. vectensis*, and changes in their expression profile were detected after exposure to UV radiation, crude oil and polycyclic aromatic hydrocarbons (Tarrant et al., 2014). A further study revealed differences in peroxide sensitivity between and within populations of *N. vectensis* (Friedman et al., 2018).

In this study, we aimed to gain first insights into the physiological importance of TRPM2 in *N. vectensis* by generating a loss-of-function mutant. We investigated whether this cation channel in *N. vectensis* is also involved in the response to oxidative stress or in the sensitivity to high temperature, despite the clear differences from the human orthologue with regard to the gating mechanism.

Our data reveal that in *N. vectensis*, TRPM2 mediates tissue damage after exposure to oxidative stress ( $H_2O_2$ ) but attenuates tissue damage after exposure to elevated (38.9°C) temperatures. These results suggest that TRPM2 plays a similar role in humans and *N. vectensis* with respect to the response to oxidative stress. In case of the responses to high-temperature stress, TRPM2 seems to have a protective function in *N. vectensis*. Thus, a direct connection between higher temperatures and oxidative stress cannot be reconciled with the functional role of TRPM2 in *N. vectensis*.

## MATERIALS AND METHODS

### *Nematostella vectensis* culture

Rearing, spawning and induction of regeneration in *Nematostella vectensis* Stephenson 1935 individuals was performed following the protocol of Stefanik et al. (2013). Adult male and female *N. vectensis* were obtained from the Cnidarian Animal Facility of Sars International Centre for Marine Molecular Biology (Bergen, Norway).

### Preparation of tissue lysates from sea anemones

Adult *N. vectensis* were relaxed in 7 mmol l<sup>-1</sup> MgCl<sub>2</sub> dissolved in *Nematostella* medium (NM, 1/3 artificial sea water; Instant Ocean). A piece of tissue a few millimetres in size, from different animals (head and physa), was dissected. The animals were pushed to the base of a Petri dish using a razorblade and tissue was dissected by cutting along the razorblade with a scalpel. Each sample that was analysed contained the pooled tissue of six different animals (three

heads and three physae). The sampled tissues were washed with PBS before an adequate volume of CellLytic MT lysis buffer (50 mg tissue sample in 1000 µl lysis buffer; Sigma-Aldrich, St Louis, MO, USA) containing 1% protease inhibitor (Sigma-Aldrich) was added. The tissue was sheared using scissors and dissociated by five 1 s sonification steps at power level two (Branson Sonifier 150, Heinemann, Schwäbisch Gmünd, Germany). After incubation for 15 min on ice, during which the samples were vortexed for 5 s every 5 min, two additional sonification steps were performed before the samples were centrifuged at 12,000 g for 15 min at 4°C. The clarified supernatant was transferred to a new tube and protein concentration was measured using Bradford reagent (Thermo Fisher Scientific, Waltham, MA, USA) according to the manufacturer's instructions. The lysates were stored at -20°C until further analysed by SDS-PAGE and western blot.

### Generation of *N. vectensis* TRPM2 loss-of-function mutants

Mutants were generated using a CRISPR-Cas9-mediated mutagenesis approach as previously described (Ikmi et al., 2014; Kraus et al., 2016). A single guide RNA (sgRNA) species was designed to target the genome region representing the central part of the pore domain of NvTRPM2. The sgRNA was synthesized using the EnGen® sgRNA Synthesis Kit, *S. pyogenes* (New England Biolabs, Ipswich, MA, USA) according to the manufacturer's instructions. For this purpose, the target-specific oligonucleotide (5'-TTCTAATACGACTACTATAGGGCGGTGTTACGATCGCGTAGTTTTAGAGCTAGA-3') was designed according to the kit manufacturer's instructions, and synthesized by Sigma-Aldrich. Fertilized *N. vectensis* eggs were dejellied with 1% cysteine (Sigma-Aldrich) dissolved in NM by shaking for 15 min. The dejellied eggs were then washed 7 times in NM. The injection mix (1 mg ml<sup>-1</sup> Cas9 endonuclease, Alexa fluorescent dye dissolved in 1.1 mol l<sup>-1</sup> KCl, 450 ng sgRNA and H<sub>2</sub>O up to total volume of 4 µl) was prepared and pre-warmed for 5 min to 37°C. Microinjection was performed using a Femtojet microinjector on a Nikon TE2000-S inverted microscope until the first cleavage of the eggs occurred. The injected animals (F<sub>0</sub> generation) were grown to sexual maturity and crossed with wild-type animals to obtain a heterozygous F<sub>1</sub> generation. These animals were screened by genomic sequencing for the presence of NvTRPM2 mutations. Female and male animals containing the same NvTRPM2 mutation were crossed to generate homozygous NvTRPM2 knockout animals (F<sub>2</sub> generation). These animals were screened by genomic sequencing and for further analysis separated according to their NvTRPM2 genotype (homozygous wild-type, heterozygous mutant, homozygous mutant). The mutant *NvTRPM2* allele used in this study was designated *NvTRPM2*<sup>1016Stop</sup> (see Results for explanation).

### Extraction, purification and sequencing of genomic DNA

Tissue of the putatively mutated animals was dissected, and extraction of the genomic DNA was performed by addition of 200 µl ethanol (100%), vortexing and incubation for 5 min. After a short centrifugation step in a table centrifuge at 6000 g, the supernatant was discarded, and the sample pellet was dried with the lid open for 45 min at 50°C in a PCR machine. Subsequently, 20–50 µl of yDNA buffer (10 mmol l<sup>-1</sup> TrisHCl, 1 mmol l<sup>-1</sup> EDTA, 25 mmol l<sup>-1</sup> NaCl) supplemented with freshly prepared proteinase K (200 µg µl<sup>-1</sup>; New England Biolabs) was added. The mixture was vortexed and incubated for 2 h at 50°C and then 10 min at 98°C. Thereafter, the samples were briefly centrifuged in a table centrifuge (6000 g) and the supernatant containing the genomic DNA was transferred to a new tube and stored at -20°C. The DNA region of the genome targeted by CRISPR-Cas9/sgRNA was

amplified by PCR using a sense and an antisense primer which bind upstream and downstream of the target region, respectively. The following primers were synthesized (Sigma-Aldrich): forward (sense) primer: 5'-CGCTCGTGGTGTGTGTTT-3'; reverse (antisense) primer: 5'-GTCGAATCAGCGCACGAGATTCAC-3'. For PCR, the Q5 high-fidelity PCR kit (New England Biolabs) was used according to the manufacturer's instructions. The temperature protocol included initial denaturation for 1 min at 98°C, followed by 40 cycles with a denaturation step for 15 s at 98°C, annealing for 30 s at 72°C and extension for 150 s at 72°C. After a final extension for 10 min at 72°C, the PCR product was cooled to 4°C. For purification, the PCR product was subjected to agarose (0.8%) gel electrophoresis and the expected DNA fragment was isolated by gel extraction (QIAquick Gel Extraction Kit, Qiagen, Hilden, Germany), according to the manufacturer's instructions. The purified DNA fragment was sequenced using the original PCR forward primer (Sigma-Aldrich).

### Molecular cloning, cell culture and transfection

The cDNA of *N. vectensis* TRPM2 (*NvTRPM2*) with codon usage adapted for heterologous expression in human cells was sub-cloned as previously described (Kühn et al., 2015). Site-directed mutagenesis (QuikChange mutagenesis system, Agilent, Santa Clara, CA, USA) was performed according to the manufacturer's instructions in order to reproduce the *NvTRPM2*<sup>1016Stop</sup> mutation for *in vitro* analysis. For immunohistological analysis of western blots or biotinylation assays in control experiments, variants of wild-type *NvTRPM2* and *NvTRPM2*<sup>1008Stop</sup> were generated that contained a triple haemagglutinin (3×HA) tag at the C-terminus (previously described in Kühn et al., 2016). All mutations and sequence manipulations were verified by DNA sequencing (Eurofins Scientific, Luxembourg, Luxembourg). Human embryonic kidney (HEK-293) cells were obtained from the German Collection of Microorganisms and Cell Cultures (Braunschweig, Germany), and authenticated and tested for contamination. Cell culture and heterologous expression of *NvTRPM2* or *NvTRPM2*<sup>1008Stop</sup> channels in HEK-293 cells using transient transfection of the corresponding cDNA was performed as previously described (Kühn et al., 2019).

### Cell surface biotinylation and western blot analysis

The biotinylation assays and western blots of heterologously transfected HEK-293 cells were performed as described previously (Kühn et al., 2019). For preparation of the membrane fraction from cell material of *N. vectensis* we used a differential centrifugation protocol previously established by Vriens et al. (2005). A primary monoclonal mouse anti-HA tag (1:1000; cat. no. H3663, Sigma-Aldrich) and mouse anti-β-actin (1:1000; cat. no. 8H10D10; Cell Signaling) were used in combination with rabbit anti-mouse HRP-conjugated secondary antisera (1:1000; cat. no. P0261, DAKO, Agilent). For western blot analysis of *NvTRPM2* expression *in vitro*, different monoclonal rabbit anti-*NvTRPM2* antisera (1:100; Davids Biotechnology, Regensburg, Germany) were used. The antiserum designated as 'type N2' was directed against the N-terminus-specific epitope (EDEVRAKVVVEVFGAKGADK) of the *NvTRPM2* protein. For western blot analysis of NUDT9 expression *in vivo*, a mouse anti-human NUDT9 antiserum (1:500; cat. no. TA503235; Origene, Rockville, MD, USA) was used. As secondary antisera, either swine anti-rabbit HRP-conjugated (1:1000; cat. no. P0217; DAKO, Agilent) or rabbit anti-mouse HRP-conjugated (1:1000; cat. no. P0261; DAKO, Agilent) antisera were used. Detection of the HRP-conjugated secondary antisera was performed using Intas

Infinity ECL Starlight (Intas Science Imaging Instruments, Göttingen, Germany) and ChemoStar Touch (Intas Science Imaging Instruments) imaging system.

### Electrophysiology

HEK-293 cells, heterologous expressing wild-type *NvTRPM2* (control) or *NvTRPM2*<sup>1008Stop</sup> channel variant, were stimulated with ADPR and Ca<sup>2+</sup> and examined by whole-cell patch-clamp analysis as described elsewhere (Kühn et al., 2019).

### Immunofluorescence confocal microscopy

Embryos (blastula to 4-tentacle polyp stage) were relaxed in 7 mmol l<sup>-1</sup> MgCl<sub>2</sub> in NM for 10 min and fixed for 30 min in ice-cold Lavdovsky Fixative (50% ethanol, 3.7% paraformaldehyde, 4% acetic acid in H<sub>2</sub>O) at 4°C. The animals were washed 3 times for 10 min, first in PBS with 0.1% Tween 20 (0.1% PBST), then in 0.1% PBST and 0.1% Triton X-100, and finally in 0.1% PBST on a shaker at room temperature (RT). The embryos were incubated overnight at 4°C with our N-terminus-specific rabbit anti-*NvTRPM2* antiserum type N2 (as described above), diluted 1:200 in 0.5% skimmed milk powder and 0.1% PBST. After three washing steps for 10 min in 0.1% PBST, the embryos were incubated for 2.5 h at RT in the dark with goat anti-rabbit secondary antiserum coupled to an Alexa 488 fluorescent dye (1:400 dilution in 0.5% skimmed milk powder and 0.1% PBST cat. no. A11034; DAKO, Agilent). Finally, embryos were incubated for 5 min at RT in the dark with Hoechst (1:10,000 diluted from stock solution 1 μg ml<sup>-1</sup> in PBS; Thermo Fisher Scientific, Waltham, MA, USA) and mounted on glass slides using Fluoromount-G mounting solution (SouthernBiotech, Birmingham, AL, USA). For imaging, a Zeiss LSM 700 confocal microscope (software version ZEN 2011 SP7 FP3) was used.

### Temporary treatment with H<sub>2</sub>O<sub>2</sub>

Individual 4-tentacle polyps of wild-type and *NvTRPM2*<sup>1016Stop</sup> animals were transferred in single wells of 6-well plates. The animals were incubated with 0.00025% H<sub>2</sub>O<sub>2</sub> in NM for 5 h under standard culture conditions (18°C in the dark). Then, H<sub>2</sub>O<sub>2</sub> was washed out with NM, and the animals were returned to standard culture conditions. As negative controls, wild-type and *NvTRPM2*<sup>1016Stop</sup> 4-tentacle polyps were treated in the same manner but without H<sub>2</sub>O<sub>2</sub> treatment. The 4-tentacle polyps were held in a relaxed state by incubation with 7 mmol l<sup>-1</sup> MgCl<sub>2</sub> in NM and bright-field images were taken, using a Nikon Eclipse Ts2 microscope and a Nikon DS-Fi3 camera at the following time points: before and 1, 2, 3 and 15 days after H<sub>2</sub>O<sub>2</sub> treatment. Different degrees of tissue damage were observed after H<sub>2</sub>O<sub>2</sub> treatment and further analysed by phalloidin staining (as described below), in order to identify effects on the muscle system. By evaluating the observed effects on overall morphology and integrity of the muscular system, we established two different categories, detailed within the Results, and distinguish between 'mild' and 'severe' tissue damage.

The treated animals were classified in the different categories and the frequency of animals displaying mild or severe tissue damage was compared between wild-type and *NvTRPM2*<sup>1016Stop</sup> animals. Six animals of each genotype were examined in each experiment, and a total of 10 such experiments were performed (altogether, 60 animals of each genotype were analysed).

### Temporary exposure to high temperature

The experimental design was similar to that used for the treatment with H<sub>2</sub>O<sub>2</sub>. Individual 4-tentacle polyps of wild-type and

NvTRPM2<sup>1016Stop</sup> animals were transferred to 0.2 ml PCR tubes and incubated at 38.9°C for 6 h in a PCR machine. Then, the animals were returned to standard culture conditions. As negative controls, wild-type and NvTRPM2<sup>1016Stop</sup> 4-tentacle polyps were treated in the same manner but without the high-temperature treatment. The animals were relaxed with 7 mmol l<sup>-1</sup> MgCl<sub>2</sub> in NM and bright-field images were taken before and 1, 2, 3 and 15 days after high-temperature treatment. The bright-field images and phalloidin staining of the high-temperature-treated animals showed similar degrees of tissue damage to that of animals in the H<sub>2</sub>O<sub>2</sub> treatment. Therefore, the same categories of tissue damage were applied to compare the effects of high-temperature treatment between wild-type and NvTRPM2<sup>1016Stop</sup> animals. Six animals of each genotype were examined in each experiment, and a total of 10 of such experiments were performed (altogether, 60 animals of each genotype were analysed).

### Phalloidin staining

Animals displaying different categories of tissue damage after treatment with H<sub>2</sub>O<sub>2</sub> or high temperature were analysed by phalloidin staining to identify effects on the muscle system. For this purpose, treated animals as well as control wild-type and NvTRPM2<sup>1016Stop</sup> animals were relaxed in 7 mmol l<sup>-1</sup> MgCl<sub>2</sub> in NM and fixed overnight at 4°C in ice-cold fixing solution (3.7% paraformaldehyde, PBS with 0.1% Tween 20). The next day, the samples were washed in PBTX (PBS with 0.2% Triton X-100) for 2 h. Every 0.5 h, the washing solution was exchanged. Then, the samples were incubated overnight at 4°C in the dark in Alexa Fluor 555 phalloidin (1:100 in PBTX, from 66 µmol l<sup>-1</sup> stock solution; Invitrogen, Thermo Fisher Scientific). After three washing steps each for 5 min in PBTX the DNA of the samples was stained for 5 min at room temperature in the dark by incubation with Hoechst 33342 (1:1000 from 1 µg ml<sup>-1</sup> stock solution in PBTX; Thermo Fisher Scientific). The samples were washed 2 times for 10 min in PBTX and mounted on glass slides using Fluoromount-G mounting solution (SouthernBiotech). Finally, the slides were dried at RT overnight in the dark and stored at 4°C. Imaging was performed with a Zeiss LSM 700 confocal microscope (software version ZEN 2011 SP7 FP3).

### Data analysis and statistics

The data for H<sub>2</sub>O<sub>2</sub> and high-temperature stress tests were analysed using GraphPad PRISM software and are expressed as means ±s.e.m. Statistical comparisons were performed using a two-way ANOVA and Fisher's LSD *post hoc* test. Differences were considered significant at \**P*<0.005.

## RESULTS

### Generation of TRPM2 mutants in *N. vectensis*

To study the physiological role of NvTRPM2 *in vivo*, an NvTRPM2 mutant was generated in *N. vectensis* using the CRISPR-Cas9 mutagenesis method. We designed an sgRNA targeting the central part of the pore domain of NvTRPM2 (Fig. 1A). The CRISPR-Cas9/sgRNA-injected animals (F<sub>0</sub> generation) were grown to sexual maturity and crossed with wild-type animals. Genomic DNA sequencing of tissue from individuals of the F<sub>1</sub> generation confirmed the presence of a 2 bp deletion inducing a frameshift mutation at the target site and two premature stop codons in the downstream open reading frame (Fig. 1B). As a result, the truncated channel variant should have neither an intact pore nor downstream protein sequences, and therefore most probably should be non-functional. We refer to this allele as NvTRPM2<sup>1016Stop</sup>, indicating the predicted premature termination of translation after amino acid 1016.

In a next step, F<sub>1</sub> animals with the corresponding (−2 bp) frameshift mutation were crossed to generate F<sub>2</sub> offspring. Tissue from the resulting F<sub>2</sub> animals again was subjected to genotyping and revealed the whole spectrum of possible genotypes with homozygous wild-type as well as heterozygous and homozygous NvTRPM2<sup>1016Stop</sup> mutants. Homozygous NvTRPM2<sup>1016Stop</sup> mutants were viable and did not show any obvious morphological differences compared with wild-type polyps (see below). The F<sub>2</sub> offspring were sorted according to their NvTRPM2 genotype and cultured for further analysis.

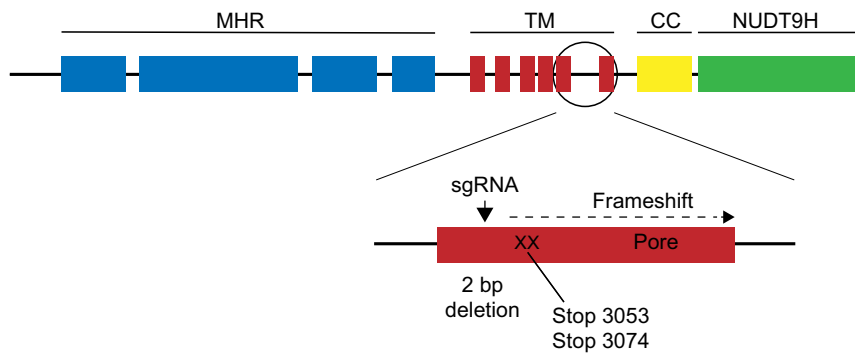
### Heterologous expression of *N. vectensis* wild-type TRPM2 and TRPM2<sup>1008Stop</sup> variant in HEK-293 cells

As no functional analysis method for the characterization of TRP channels in marine invertebrates has been established so far, we decided to test the effects of the NvTRPM2<sup>1016Stop</sup> mutation in *N. vectensis* by comparative phenotypic analysis of intact animals rather than by patch-clamp analysis or calcium imaging of single cells. For the characterization of NvTRPM2<sup>1016Stop</sup> *in vitro*, we tested surface expression as well as channel function using an established heterologous expression system of NvTRPM2 (Kühn et al., 2015). For this purpose, the corresponding frameshift mutation of the NvTRPM2<sup>1016Stop</sup> allele was reproduced *in vitro* by site-directed mutagenesis (Fig. 1C) of NvTRPM2 cDNA and analysed in comparison with wild-type NvTRPM2 expression in HEK-293 cells. For heterologous expression in HEK-293 cells, the codon usage of the synthesized open reading frame of NvTRPM2 was adapted to the human version. As a result, the induced frameshift as well as the position of the premature stop codon are not identical to the corresponding variant generated *in vivo* (Fig. 1C). However, these small differences were not considered functionally relevant. We refer to this channel variant as NvTRPM2<sup>1008Stop</sup>, indicating the slightly shifted position of the stop codon.

### Surface expression of the NvTRPM2<sup>1008Stop</sup> channel variant in HEK-293 cells

First, we analysed surface expression of the NvTRPM2<sup>1008Stop</sup> channel in transiently transfected HEK-293 cells using a commercially available cell surface biotinylation assay. Transfected cells were exposed to biotinylation and subsequently the cell lysates were examined with SDS-PAGE and western blot analysis. For effective detection in western blot analysis, we used 3×HA-tagged variants of both wild-type NvTRPM2 (positive control) and NvTRPM2<sup>1008Stop</sup> (see Materials and Methods). The anti-HA tag antisera detected clear signals in the HA-tagged samples corresponding to the calculated mass of wild-type NvTRPM2-3×HA (175 kDa) and NvTRPM2<sup>1008Stop</sup>-3×HA (115 kDa) (Fig. 2, lanes 1, 2, 4, 5). Thus, the transfection control showed strong expression of wild-type NvTRPM2 as well as NvTRPM2<sup>1008Stop</sup> channels, whereas no specific expression could be detected in mock-transfected control cells (Fig. 2, lanes 4–6). Likewise, in the biotinylated membrane fraction, the wild-type NvTRPM2 and NvTRPM2<sup>1008Stop</sup> mutant demonstrated comparable surface expression levels, whereas no signals could be detected in mock-transfected control cells (Fig. 2, lanes 1–3). Thus, despite its aberrant structure, the surface expression of the truncated NvTRPM2<sup>1008Stop</sup> protein was comparable to that of wild-type NvTRPM2. This result was not surprising because previous studies demonstrated regular surface expression of similarly truncated splice variants of HsTRPM2 (Zhang et al., 2003).

A



B

**Wild-type *NvTRPM2***

DNA 2983 TTC ACG ATC G **CG** TAC GGC ATC GCT CTG CAC GCG GTC ATG TTC CCG AGT CCT GGG  
 Protein 995 F T I A Y G I A L H A V M F P S P G

DNA ATC TAC GCC AGG AAT AAC ACG TGG GTG ACG ATC ACT ... 4656  
 Protein I Y A R N N T W V T I T ... 1551 172 kDa

***NvTRPM2*<sup>1016Stop</sup>**

DNA 2983 TTC ACG ATC **GTA CGG CAT CGC TCT GCA CGC GGT CAT GTT CCC GAG TCC TGG**  
 Protein 995 F T I **V R H R S A R G H V P E S W**

DNA **GAT CTA CGC CAG GAA TAA CAC GTG GGT GAC GAT CAC TAG** 3053/3074  
 Protein **D L R Q E stop H V G D D H stop** 1016/1023 113 kDa

C

**Wild-type *NvTRPM2***

DNA 2983 TTC ACT ATC G**CG** TAT GGA ATC GCT CTG CAT GCC GTG ATG TTC CCT AGT CCA GGC  
 Protein 995 F T I A Y G I A L H A V M F P S P G

DNA ATT TAT GCC CGC AAT AAT ACG TGG GTG ACA ATT ACA ... 4656  
 Protein I Y A R N N T W V T I T ... 1551 172 kDa

***NvTRPM2*<sup>1008Stop</sup>**

DNA 2983 TTC ACT ATC **GTA TGG AAT CGC TCT GCA TGC CGT GAT GTT CCC TAG TCC AGG**  
 Protein 995 F T I **V R N R S A C R D V P stop S R**

DNA **CAT TTA TGC CCG CAA TAA** 3027/3051  
 Protein **H L C P Q stop** 1008/1016 112 kDa

**Function of the *NvTRPM2*<sup>1008Stop</sup> channel variant in HEK-293 cells**

For functional characterization of the *NvTRPM2*<sup>1008Stop</sup> channel variant *in vitro*, we performed whole-cell patch-clamp experiments of transiently transfected HEK-293 cells. As demonstrated in Fig. 3A, wild-type *NvTRPM2* exhibited typical currents after stimulation with moderate concentrations of ADPR (0.15 mmol l<sup>-1</sup>) and Ca<sup>2+</sup> (1 μmol l<sup>-1</sup>), both applied through the pipette solution. Immediately after breaking into the cell at a holding potential of -60 mV, strong inward currents developed, reaching maximum amplitude within <5 s. Afterwards, a rapid current decline took place that reduced the current amplitude to less than 15% within 30 s. Replacement of extracellular Na<sup>+</sup> with the impermeable cation NMDG blocked the inward component of the current. In strong

contrast, no such currents could be induced when HEK-293 cells transfected with *NvTRPM2*<sup>1008Stop</sup> were stimulated with ADPR and Ca<sup>2+</sup>. Even if a very high concentration (1.25 mmol l<sup>-1</sup>) of ADPR was applied, there was no significant current response detectable (Fig. 3B). Therefore, the expression/function analysis of an almost identical channel variant *in vitro* strongly suggests that our *NvTRPM2*<sup>1016Stop</sup> mutant represents a loss-of-function allele.

**Validation of specific antisera to detect expression of *NvTRPM2* *in vitro* and *in vivo***

As no standard antisera were available as probes for *NvTRPM2*, three different antisera were produced. Most of the *NvTRPM2* protein downstream of the pore region is constituted by the NUDT9H domain, and this part is absent in the *NvTRPM2*<sup>1016Stop</sup>

**Fig. 1. Primary domain structure of full-length *NvTRPM2* and sequence manipulations required for the generation of *NvTRPM2*<sup>1016Stop</sup> *in vivo* and *in vitro*.**

(A) The principal domains are TRPM homology region (MHR), transmembrane domain (TM), coiled-coil domain (CC) and NUDT9H. A 2 bp deletion was introduced within the pore region (circled) by CRISPR-Cas9 mutagenesis. The resulting downstream (-2 bp) frameshift generates two premature stop codons (indicated by 'X'). (B,C) Corresponding DNA and amino acid sequences of the target pore region of *NvTRPM2* with modifications (in red) for expression either *in vivo* (B) or *in vitro* (heterologous expression in HEK-293 cells; C). Relative positions are given at the beginning and at the end of the sequences. The calculated mass (kDa) of the full-length wild-type channel and truncated channel variants is indicated.

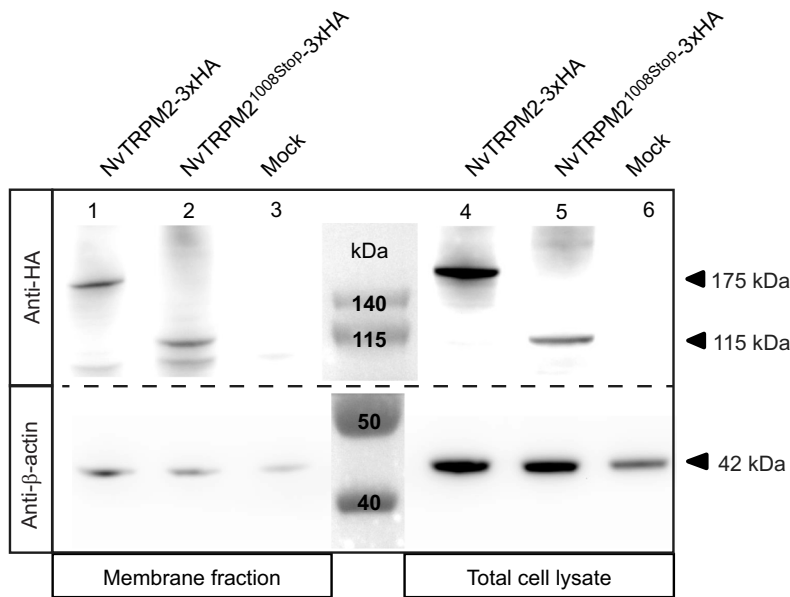


**Fig. 2. Cell surface expression of wild-type NvTRPM2 and mutant NvTRPM2<sup>1008Stop</sup> heterologously expressed in HEK-293 cells.** A standard cell surface biotinylation assay was performed with the corresponding triple haemagglutinin (3×HA)-tagged channel variants heterologously expressed in HEK-293 cells. Biotinylated cell lysates were incubated with NeutrAvidin beads and afterwards eluted with SDS-sample buffer. Eluates and the corresponding total cell lysates (as indicated) were subjected to reducing SDS-PAGE and western blot analysis. Mock-transfected cells were used as a negative control. The western blot membrane was cut between 50 and 65 kDa (indicated by the dashed line) and incubated with commercially available anti-HA and anti-β-actin antibodies. Because of different staining intensities, variable exposure times were applied for the identification of HA and β-actin signals. Three independent experiments gave similar results.

variant. For this reason, the application of C-terminus-specific anti-TRPM2 antisera would be the method of choice. However, for NvTRPM2, this strategy is hampered by the fact that the orthologue of the human NUDT9 enzyme is probably also expressed in *N. vectensis*. The genome of *N. vectensis* contains a predicted open reading frame of 281 amino acid residues that shows 45% sequence identity with the human NUDT9 enzyme (350 amino acid residues; Kühn et al., 2017). Using an antiserum against human NUDT9, we detected bands of the expected size in western blots from wild-type and NvTRPM2<sup>1016Stop</sup> animals (Fig. S1). This finding indicates that antisera against the C-terminus of NvTRPM2 most probably would cross-react with the endogenous NUDT9 orthologue of *N. vectensis*.

We therefore selected epitopes in the N-terminal part of NvTRPM2 for generation of antisera, although these epitopes would be present in both control animals and NvTRPM2<sup>1016Stop</sup>

mutants. While these antisera cannot be validated using NvTRPM2<sup>1016Stop</sup> mutants for immunofluorescence, they could in principle be validated by western blot of mutants and control animals. For this purpose, we applied a special membrane fractionation protocol using differential centrifugation (Vriens et al., 2005). This method proved successful in our laboratory for the detection of diverse heterologously expressed ion channels (Winking et al., 2012). Unfortunately, all our attempts to detect NvTRPM2 by western blot from wild-type or mutant animals failed (data not shown). Most probably, this was because only limited cell material was available for western blot analysis, resulting in an inefficient preparation of cell membranes. In addition, it cannot be ruled out that the protocol of Vriens et al. (2005) did not work with our *N. vectensis* preparations.

We next turned to the heterologous expression of NvTRPM2 in HEK-293 cells to test the specificity of our anti-NvTRPM2 antisera

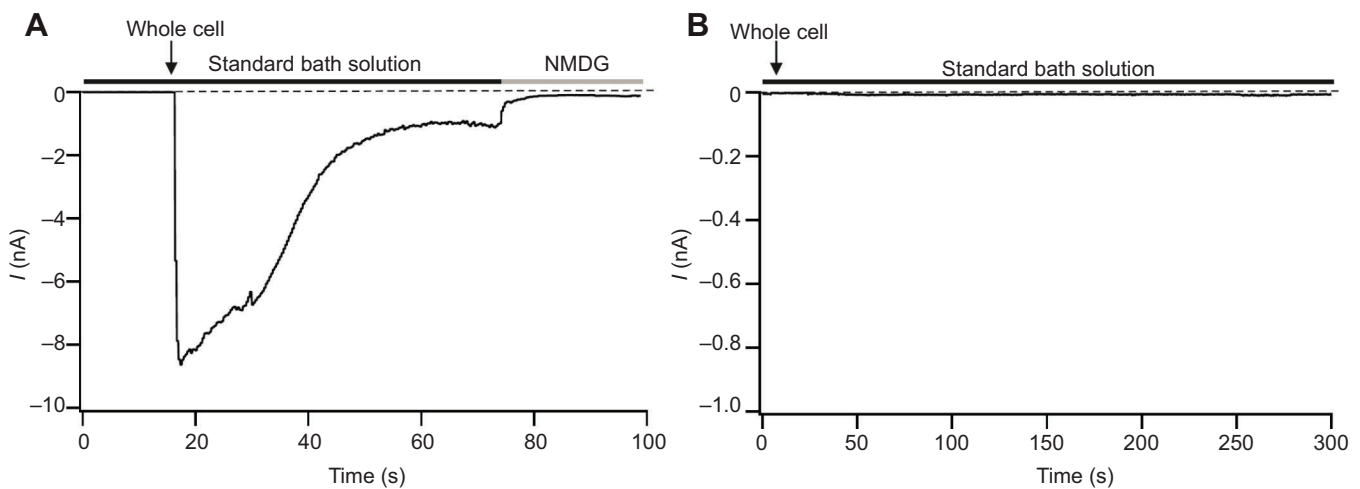


**Fig. 3. Whole-cell patch-clamp analysis of wild-type NvTRPM2 and mutant NvTRPM2<sup>1008Stop</sup> heterologously expressed in HEK-293 cells.** Transiently transfected cells were stimulated with ADPR (0.15 mmol l<sup>-1</sup> ADPR for NvTRPM2 and 1.25 mmol l<sup>-1</sup> ADPR for NvTRPM2<sup>1016Stop</sup>) and Ca<sup>2+</sup> (1 μmol l<sup>-1</sup>) applied through the patch pipette. (A) After establishment of the whole-cell configuration, wild-type NvTRPM2 showed typical current kinetics with a very fast current increase followed by a spontaneous current decline. Replacement of extracellular Na<sup>+</sup> with the impermeable cation NMDG blocked the inward currents. (B) No currents could be evoked in cells transfected with the NvTRPM2<sup>1008Stop</sup> variant, even though a very high concentration of ADPR was applied. Six independent experiments gave similar results.

in comparison to the standard anti-HA antisera. We found that, in particular, antiserum type N2 allowed specific identification of both full-length wild-type NvTRPM2 and the truncated NvTRPM2<sup>1016Stop</sup> variant (Fig. S2).

Therefore, our type N2 antiserum represents a promising tool to investigate the general expression of NvTRPM2 in *N. vectensis* in more detail.

### Analysis of NvTRPM2 expression in *N. vectensis* by immunofluorescence

Based on the data obtained from our preliminary experiments, we decided to examine the expression of wild-type NvTRPM2 in *N. vectensis* by immunofluorescence and confocal microscopy. Therefore, we used different developmental stages of *N. vectensis* that were stained for DNA (Hoechst) and NvTRPM2 (anti-NvTRPM2 antiserum type N2). As shown in Fig. 4, all analysed larval developmental stages were labelled by anti-NvTRPM2 antiserum. In the gastrula (Fig. 4A,B), the expression of NvTRPM2 was identified in two distinct locations: the numerous single round cells distributed all over the animal (arrowheads), the number of which varied in the different focal planes of the animal; and in a layer surrounding the whole gastrula and most likely representing the plasma membrane of the outer cells. The same expression profile of NvTRPM2 was detected in planula larvae (Fig. 4C). In addition, we observed positive signals in elongated cellular regions of the pharynx (Fig. 4C, arrow). However, this could be non-specific staining of cnidocytes (the capsules of stinging cells), as has been observed with other immunofluorescence probes (J.M.G. and F.R., unpublished observations). Similar potentially non-specific staining of cnidocytes was observed in juvenile polyps (Fig. 4E,F, arrow). Moreover, in juvenile polyps, the signals for expression of NvTRPM2 in individual round cells seem to be less condensed and instead more distributed over the animal. Here, the expression of NvTRPM2 in the plasma membrane was especially pronounced, showing signals in a focal plane of cells on the animal's surface (Fig. 4D). Altogether, these results indicate that the expression of NvTRPM2 is not limited to a specific larval developmental stage or distinct animal structures. Furthermore, NvTRPM2-specific signals could be detected in the plasma membrane, which is in accordance with its function as an ion channel.

### Reproduction and development of *N. vectensis* NvTRPM2 mutants under standard environmental conditions

To obtain homozygous NvTRPM2<sup>1016Stop</sup> animals, we crossed heterozygous NvTRPM2<sup>1016Stop</sup> F<sub>1</sub> animals and identified homozygous NvTRPM2<sup>1016Stop</sup> F<sub>2</sub> animals by PCR and DNA sequencing. We further in-crossed the homozygous F<sub>2</sub>s to obtain homozygous NvTRPM2<sup>1016Stop</sup> F<sub>3</sub> animals that reached the adult stage. Thus, under our culture conditions, reproduction was not impaired in the heterozygous and homozygous NvTRPM2<sup>1016Stop</sup> polyps.

Likewise, the development from fertilized eggs to adult animals was not noticeably affected in NvTRPM2<sup>1016Stop</sup> animals. The different developmental stages exhibited no visible difference from wild-type animals, and we did not observe a delay in development (Fig. S3). The fertilized eggs developed first into blastulae, which then underwent gastrulation by invagination (Kraus and Technau, 2006; Magie et al., 2007). Afterwards, the animals elongated into a free-swimming planula larvae with a tuft of long cilia at the aboral pole. The animals elongated further, and first tentacle buds arose. Finally, by elongation of the body and tentacles, the 4-tentacle polyp stage was reached.

From then, growth beyond the 4-tentacle polyp stage depended on nutritional status (Ikmi et al., 2020). Regular feeding of wild-type and NvTRPM2<sup>1016Stop</sup> animals led to adult individuals that did not differ in appearance.

In summary, neither reproduction nor development of *N. vectensis* from fertilized eggs to the adult stage was significantly impaired by the mutation of NvTRPM2.

### Phenotypic characterization of NvTRPM2 mutant animals under oxidative stress conditions

In humans, there is ample evidence for a central role of TRPM2 in oxidative stress-mediated apoptosis (e.g. Malko and Jiang, 2020). Accordingly, in transiently transfected HEK-293 cells, the human TRPM2 channel can be readily activated by extracellular application of H<sub>2</sub>O<sub>2</sub> (Hara et al., 2002; Wehage et al., 2002). For NvTRPM2, however, under the same experimental conditions the sensitivity to H<sub>2</sub>O<sub>2</sub> strongly depends on the catalytic activity of the endogenous NUDT9H domain (Kühn et al., 2016, 2019). It is therefore possible that in *N. vectensis*, the NvTRPM2 channel is also involved in the responses to oxidative stress, but this process might be differently regulated, when compared with mammalian cells.

Intraspecific variation in the sensitivity to H<sub>2</sub>O<sub>2</sub> of different populations of *N. vectensis* was discovered in a previous study (Friedman et al., 2018), using concentrations of H<sub>2</sub>O<sub>2</sub> between 0.00025% and 0.0005% continuously applied throughout the experiments. In our study, we decided to analyse the physiological role of NvTRPM2 in the response to oxidative stress *in vivo* by transient (5 h) incubation of primary polyps (4-tentacle polyps) in 0.00025% H<sub>2</sub>O<sub>2</sub>. In our preliminary experiments, this concentration, as well as the transient incubation, were found to induce tissue damage without killing most animals tested. Thus, our H<sub>2</sub>O<sub>2</sub> treatment was effective but not lethal. For more details on the treatment with H<sub>2</sub>O<sub>2</sub> as well as the procedures to categorize the resulting tissue damage, see Materials and Methods. The treated animals of both genotypes were analysed for signs of tissue damage at selected times after transient exposure to H<sub>2</sub>O<sub>2</sub>. The applied time course of 1, 2, 3 and 15 days was used because *N. vectensis* shows fast body regeneration after injury, i.e. in the analysed time period, we wanted to exclude significant attenuation of stress-induced lesions by regeneration effects.

Representative images demonstrating the effect of H<sub>2</sub>O<sub>2</sub> treatment on wild-type and NvTRPM2<sup>1016Stop</sup> 4-tentacle polyps are given in Fig. 6. In control animals, both body column and tentacles were extended and the mesenteries were visible in the gastrovascular cavity with some distance to the tissue of the body column (Fig. 5A). After H<sub>2</sub>O<sub>2</sub> treatment, different degrees of tissue damage were observed in wild-type as well as in NvTRPM2<sup>1016Stop</sup> animals. Whereas some animals suffered minor damage, others were completely dissociated (Fig. 5C versus E and G). Most of the H<sub>2</sub>O<sub>2</sub>-treated animals showed pronounced body shrinking with mesenteries and gastrovascular cavity being invisible. Additionally, the length of the tentacles was strongly decreased. While some of the treated animals recovered to some extent over time, others deteriorated further and finally dissociated completely (Fig. 5E,G).

To get more insight into the induced damage at the tissue level, we performed confocal microscopy after staining tissues with phalloidin coupled to a fluorescent dye (Fig. 5, right). In this way, filamentous actin structures were made visible, which mainly belong to the muscle system of *N. vectensis*. This muscle system consists of longitudinal retractor muscles in the tentacles, longitudinal retractor muscles in the mesenteries (infoldings of the body column endoderm), and longitudinal parietal muscles and

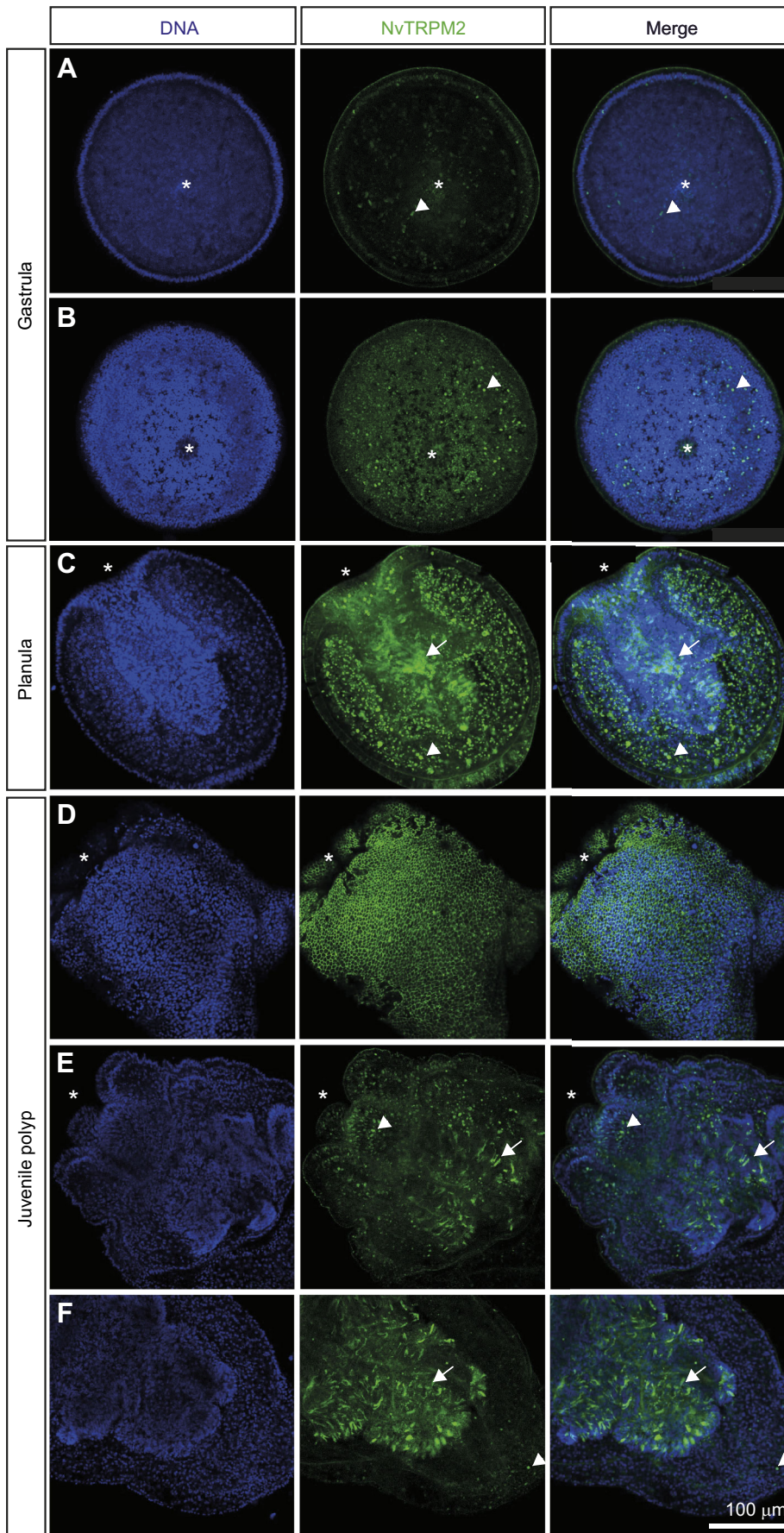


**Fig. 4. Representative immunofluorescence images showing expression of wild-type NvTRPM2 in distinct developmental stages of *Nematostella vectensis*.** Different developmental stages of *N. vectensis* (as indicated) were stained for DNA with Hoechst and probed with our specific anti-NvTRPM2 antiserum targeting an N-terminal epitope of NvTRPM2. The blastopore (site of future mouth) is marked by an asterisk. (A,B) For the gastrula stage, two different focal planes of the same animal are shown. (C) Planula stage. (D–F) For the juvenile polyp stage, D and E represent two different focal planes of different animals, and E and F represent different areas of the same animal at the same focal plane. In all developmental stages tested, a distinct expression pattern of NvTRPM2 was detected. This includes single cells distributed all over the organisms (indicated with arrowheads) as well as the plasma membrane (gastrula, planula and juvenile polyp; A–D). Positive signals were also detected in cnidocysts (indicated by arrows) but most likely were non-specific (J.M.G. and F.R., unpublished observations). Ten experiments with 15 individual animals in each experiment gave similar results. Images were taken with a confocal microscope at 40 $\times$  resolution and show the different channels for DNA and NvTRPM2 signals and the merge of the channels. For better visibility, the brightness of the images was adjusted to +40%. Scale bar: 100  $\mu$ m (applies to all images).



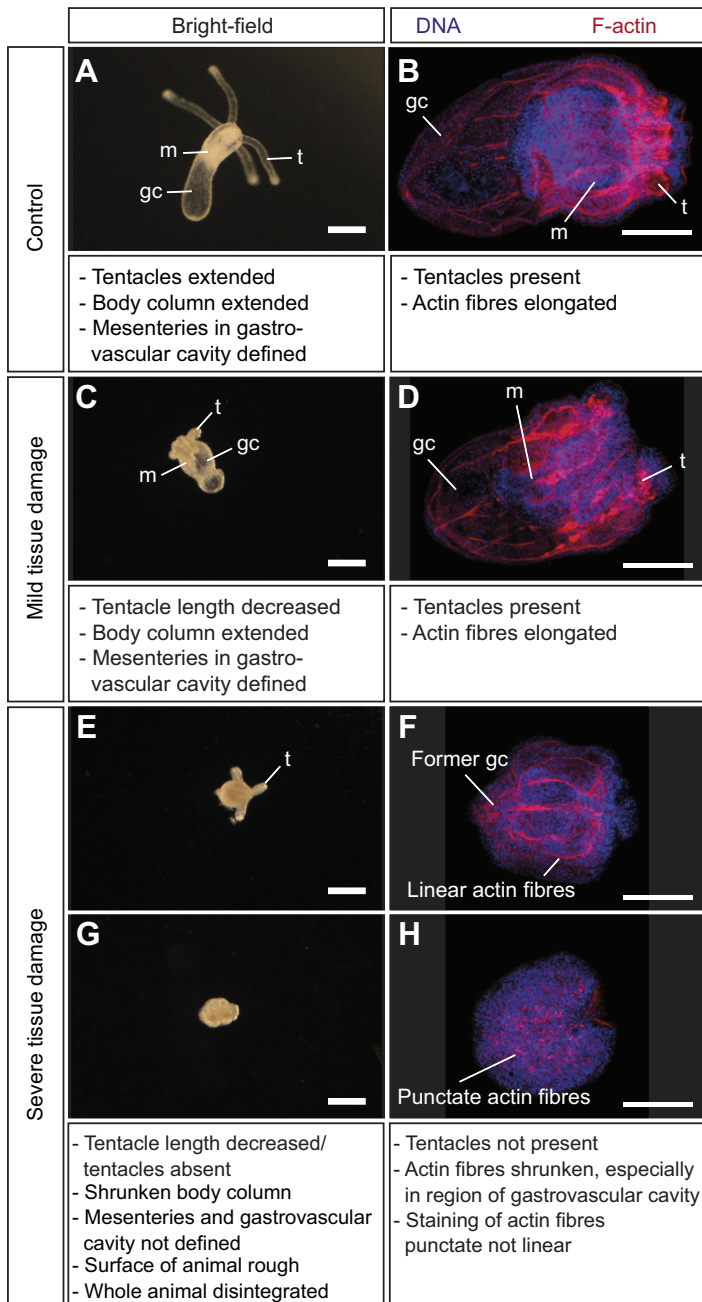


**Fig. 5. Classification of the degree of H<sub>2</sub>O<sub>2</sub>-induced tissue damage in 4-tentacle polyps of wild-type and NvTRPM2<sup>1016Stop</sup> animals.**

*Nematostella vectensis* were transiently incubated for 5 h with 0.00025% H<sub>2</sub>O<sub>2</sub>. Bright-field microscopy images of the animals were taken before and 1, 2, 3 and 15 days after H<sub>2</sub>O<sub>2</sub> treatment (left). Actin fibres were stained with phalloidin coupled to fluorescent dye Alexa 555 to analyse the effect of H<sub>2</sub>O<sub>2</sub> treatment on the muscle system (actin fibres) of the animals (right). Tissue damage in treated animals was classified as 'mild' or 'severe'; animals with mild tissue damage looked similar to the untreated control animals. In corresponding bright-field images, tentacles were present, mesenteries were visible within the gastrovascular cavity and the body column was elongated (A,C). Phalloidin staining revealed staining of tentacle muscles and linear actin fibres that extend along the oral–aboral body axis (B,D). Animals that displayed severe tissue damage had very short or absent tentacles and a shrunken body column. The mesenteries were not visible within the gastrovascular cavity and some animals had completely disintegrated (E,G). Phalloidin staining revealed shrunken actin fibres, especially in the region of the former gastrovascular cavity, and less or no staining of tentacle muscles (F,H). Some animals showed no linear actin fibre staining, only punctate, indicating a process of disintegration of inner muscle structures (H). Five experiments with 15 individual animals in each experiment gave similar results. Important animal tissue structures are indicated: t, tentacles; m, mesenteries; gc, gastrovascular cavity. Scale bars: 100 µm.

circumferential ring muscle, both located in the body column (Jahnel et al., 2014). Therefore, we used the results of our phalloidin staining experiments to refine our observations of the living polyps.

The phalloidin staining of control and H<sub>2</sub>O<sub>2</sub>-treated animals revealed clear differences in the structure of actin fibres (Fig. 5). In control animals, longitudinal actin fibres of the body column were observed extending along the oral–aboral axis and the gastrovascular cavity was visible. The actin fibres within the tentacles were also visible near the oral opening (Fig. 5B). In contrast, H<sub>2</sub>O<sub>2</sub>-treated animals more often displayed small changes of actin fibres. The length of the actin fibres was slightly reduced in the shrunken tentacles and the gastrovascular cavity (Fig. 5D). Moreover, some H<sub>2</sub>O<sub>2</sub>-treated animals also showed strongly truncated actin fibres within the shrunken tentacles or even the complete absence of actin fibres and tentacles. The originally elongated longitudinal actin fibres of the body column were

contracted so that the gastrovascular cavity was constricted (Fig. 5F,H). In some of these animals, the signals for actin fibres were no longer linear (an indication of elongated actin fibres); instead, only punctate actin fibre signals could be detected (Fig. 5H). This observation points to a severe perturbation of the animal's muscular system.

Animals of both genotypes displayed the same spectrum of possible tissue damage, and all H<sub>2</sub>O<sub>2</sub>-treated animals were assigned to one of the two categories of tissue damage: mild or severe. We compared the frequency of occurrence of the two categories of tissue damage between wild-type and NvTRPM2<sup>1016Stop</sup> animals (Fig. 6). In total, 60 animals of each genotype were analysed, and 15 days after H<sub>2</sub>O<sub>2</sub> treatment the proportion of NvTRPM2<sup>1016Stop</sup> animals displaying a mild degree of H<sub>2</sub>O<sub>2</sub>-induced tissue damage was significantly increased (60% of all analysed NvTRPM2<sup>1016Stop</sup> animals), compared with wild-type (35% of all analysed wild-type

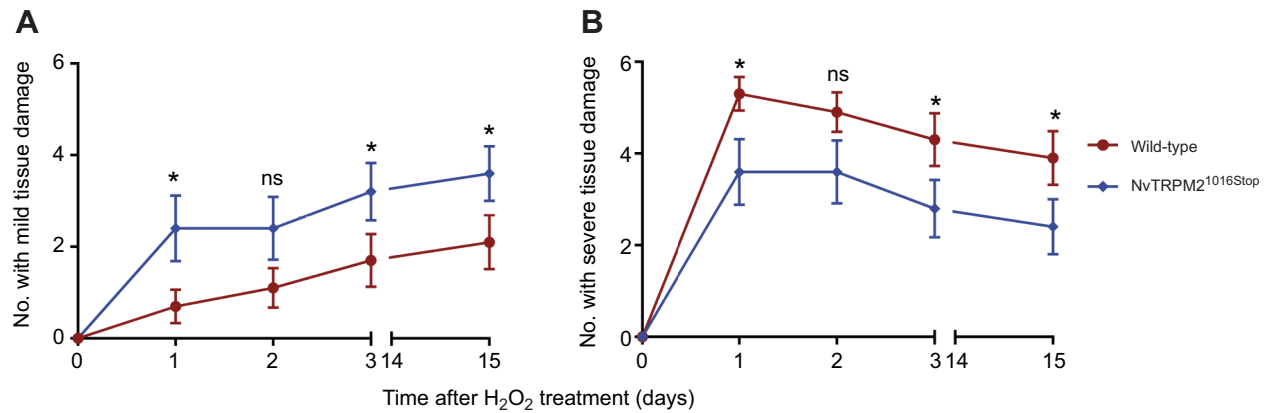


**Fig. 6. Effect of H<sub>2</sub>O<sub>2</sub>-induced tissue damage on 4-tentacle polyps of wild-type and NvTRPM2<sup>1016Stop</sup> animals.** *Nematostella vectensis* were transiently incubated for 5 h in NM supplemented with 0.00025% H<sub>2</sub>O<sub>2</sub> under standard culture conditions (18°C in the dark). Bright-field images were taken, and the degree of tissue damage was scored before treatment and 1, 2, 3 and 15 days after exposure to H<sub>2</sub>O<sub>2</sub>. For each experiment, 6 wild-type and 6 NvTRPM2<sup>1016Stop</sup> animals were analysed, and this experimental setting was repeated 10 times, so in total 60 animals of each genotype were analysed. The number of animals with mild (A) or severe (B) tissue damage was significantly different between NvTRPM2<sup>1016Stop</sup> and wild-type animals. Data are means±s.e.m.; statistical analysis was performed with a two-way ANOVA ( $n=10$ , significant difference between genotypes  $P=0.0005$  and time after treatment  $P<0.0001$ ) and Fisher's LSD *post hoc* test (\* $P<0.005$ ; ns, not significant).

animals) animals (Fig. 6A). In contrast, the number of animals displaying a severe degree of H<sub>2</sub>O<sub>2</sub>-induced tissue damage was significantly decreased in NvTRPM2<sup>1016Stop</sup> (40% of all analysed NvTRPM2<sup>1016Stop</sup> animals), compared with wild-type (65% of all analysed wild-type animals) animals (Fig. 6B). These data strongly suggest that in *N. vectensis*, the NvTRPM2 channel participates in the response to oxidative stress most likely by mediating tissue damage. Consequently, NvTRPM2 channels must be sensitive to H<sub>2</sub>O<sub>2</sub> *in vivo* and, on the basis of the divergent *in vitro* data (Kühn et al., 2015, 2016, 2019), need to be regulated in some way in *N. vectensis*.

#### Phenotypic characterization of the NvTRPM2 mutant animals under conditions of high temperatures

Substantial fluctuations in water temperature are a hallmark of the natural habitat of *N. vectensis*. Furthermore, it was demonstrated that for marine invertebrates, higher water temperatures are intimately related to conditions of oxidative stress (Shedder et al., 1997; González Durán et al., 2019).

The human TRPM2 orthologue was shown to be directly activated by temperatures that are in the range of our applied stress-test temperature (Tan and McNaughton, 2016; Song et al., 2016; Kashio and Tominaga, 2017). Therefore, we wanted to test whether mutation of NvTRPM2 also affects high-temperature-induced injury in *N. vectensis*. For this purpose, we analysed the effects of high temperature (38.9°C) on the phenotype of wild-type and NvTRPM2<sup>1016Stop</sup> animals using a similar design to the H<sub>2</sub>O<sub>2</sub> exposure experiment. Intraspecific variation in temperature sensitivity of different populations of *N. vectensis* has been described in the literature (Reitzel et al., 2013), with all developmental stages having critical temperatures within 1°C (39.5–40.5°C). In preliminary experiments, we found that incubation at 38.9°C for 6 h was effective but not lethal and therefore we performed the experiments at this temperature. For more details of the exposure to high temperature as well as the procedures to categorize the resulting tissue damage, see Materials and Methods. In total, 60 animals of each genotype, both wild type and NvTRPM2<sup>1016Stop</sup>, were analysed and the different degrees of tissue damage that were induced after high-temperature stress corresponded to those observed after treatment with H<sub>2</sub>O<sub>2</sub>.

Consequently, we used the same categories to estimate the effects on tissue damage.

Before starting the experiment, animals were in an extended state with phenotypical characteristics as described before. Likewise, the occurrence and specific distribution of high-temperature-induced tissue damage were similar to those observed after exposure to oxidative stress. However, the relative effects of temperature stress on wild-type and NvTRPM2<sup>1016Stop</sup> polyps turned out to be the opposite of those induced by oxidative stress. The experimental data revealed that 15 days after high-temperature treatment, the number of animals displaying a mild degree of tissue damage was significantly decreased in NvTRPM2<sup>1016Stop</sup> (27% of all analysed NvTRPM2<sup>1016Stop</sup> animals) when compared with wild-type (45% of all analysed wild-type animals) animals (Fig. 7A). In contrast, the portion of animals displaying a severe degree of H<sub>2</sub>O<sub>2</sub>-induced tissue damage was significantly increased in NvTRPM2<sup>1016Stop</sup> (73% of all analysed NvTRPM2<sup>1016Stop</sup> animals) compared with wild-type (55% of all analysed wild-type animals) animals (Fig. 6A). Thus, it seems that NvTRPM2 does not mediate high-temperature stress but protects sea anemones from harmful effects induced by this stressor.

#### DISCUSSION

Our comparative analysis of the phenotypes of wild-type and NvTRPM2<sup>1016Stop</sup> animals reveals that NvTRPM2 mediates tissue damage in *N. vectensis* after exposure to oxidative stress. The observed injuries after temporary treatment with 0.00025% H<sub>2</sub>O<sub>2</sub> were significantly reduced in the NvTRPM2<sup>1016Stop</sup> animals compared with wild-type animals. Using phalloidin staining, we could show that in damaged tissues the actin fibres of the cytoskeleton were strongly impaired. This disintegration of intracellular structures might point to apoptosis, which would be in line with the data obtained from the human TRPM2 orthologue (e.g. Yamamoto et al., 2008; Uchida et al., 2011; Miller and Cheung, 2016). However, while in human cells TRPM2 can be readily stimulated with H<sub>2</sub>O<sub>2</sub> both *in vitro* and *in vivo* (Perraud et al., 2005; Fonfria et al., 2005; Buelow et al., 2008; Hara et al., 2002; Hecquet et al., 2014), this is not the case for NvTRPM2 during heterologous expression in HEK-293 cells (Kühn et al., 2015, 2016, 2019). Most probably, this is caused by the NUDT9H domain of

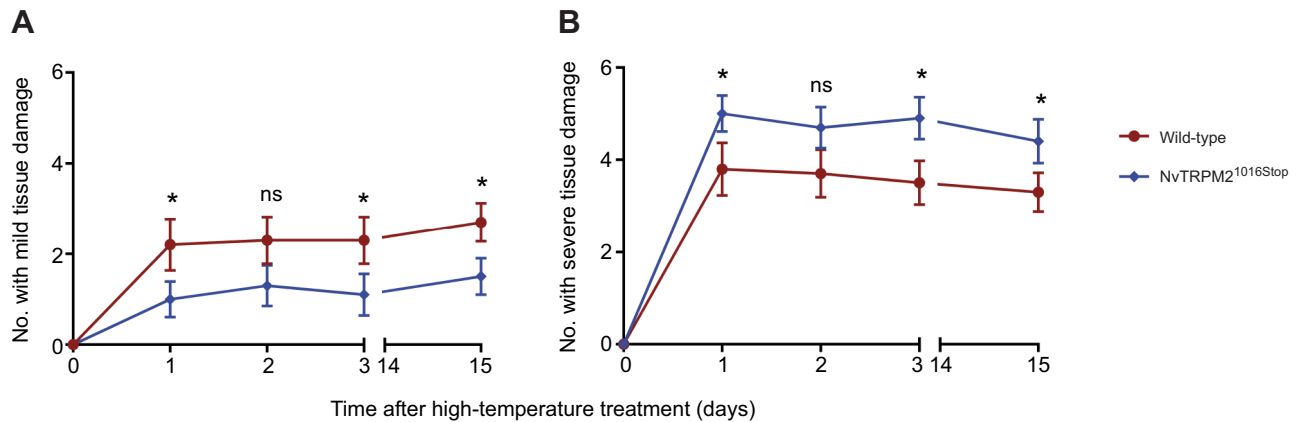


**Fig. 7. Effect of high-temperature-induced tissue damage on 4-tentacle polyps of wild-type and NvTRPM2<sup>1016Stop</sup> animals.** *Nematostella vectensis* were incubated for 6 h in NM at 38.9°C using a PCR machine and afterwards returned to standard culture conditions (18°C in the dark). Bright-field images were taken, and the degree of tissue damage was scored before treatment and 1, 2, 3 and 15 days after high-temperature treatment. For each experiment, 6 wild-type and 6 NvTRPM2<sup>1016Stop</sup> animals were analysed, and this experimental setting was repeated 10 times, so in total 60 animals of both genotypes were analysed. The number of animals with mild (A) or severe (B) tissue damage was significantly different between NvTRPM2<sup>1016Stop</sup> and wild-type animals. Data are means ± s.e.m.; statistical analysis was performed with a two-way ANOVA ( $n=10$ , significant difference between genotypes  $P=0.0008$  and time after treatment  $P<0.0001$ ) and Fisher's LSD *post hoc* test (\* $P<0.005$ ; ns, not significant).

NvTRPM2, as suppression of its ADPRase function *in vitro* leads directly to the sensitization of the channel to H<sub>2</sub>O<sub>2</sub> (Kühn et al., 2016, 2017, 2019).

Oxidative stress in the form of reactive oxygen species can be generated both inside the cell, e.g. as by-products of an (inadequate) respiratory chain, and through external environmental influences on the organism. The applied concentration of 0.00025% (82 μmol l<sup>-1</sup>) H<sub>2</sub>O<sub>2</sub> in our experiments is within the range of concentrations used in another study which examined intraspecific variation in oxidative stress tolerance of adult *N. vectensis* (Friedman et al., 2018). In the same study, it was shown that continuous incubation with twice the concentration (0.0005%) of H<sub>2</sub>O<sub>2</sub> leads to a drastic increase in the mortality rate of adult animals, which reaches almost 100% with a further increase in concentration (Friedman et al., 2018). In contrast, in our comparative stress test analysis, we used primary polyps (4-tentacle polyps) instead of adult animals of *N. vectensis*, and both the applied concentration and the exposure time of H<sub>2</sub>O<sub>2</sub> treatment were adjusted to a sub-lethal range. Remarkably, for the extracellular stimulation of TRPM2 in transfected HEK-293 cells, bolus concentrations of H<sub>2</sub>O<sub>2</sub> in the high micromolar to millimolar range are necessary (Bari et al., 2009; Zou et al., 2013). This usually induces strong channel activation and subsequently cellular apoptosis within a few minutes (e.g. Wehage et al., 2002; Sun et al., 2012). It is very likely that only a fraction of this extracellular bolus addition will be effective inside the cell because various cytosolic enzymes rapidly decompose H<sub>2</sub>O<sub>2</sub>. For the same reason, the effective concentrations of H<sub>2</sub>O<sub>2</sub> *in vivo* are difficult to estimate, especially as extracellular bolus addition of H<sub>2</sub>O<sub>2</sub> does not lead to a uniform spatiotemporal distribution of H<sub>2</sub>O<sub>2</sub> throughout the cell (Lim et al., 2016).

According to a previous study, our applied concentration of H<sub>2</sub>O<sub>2</sub> is in the upper range of levels recorded in aquatic environments comparable to the natural habitat of *N. vectensis* (Abele-Oeschger et al., 1997).

Notably, oxidative stress stimulates TRPM2 in an indirect manner and channel activation represents only one of several steps in the pathway of cellular apoptosis (Perraud et al., 2005; Pascal and Ellenberger, 2015). In the case of *N. vectensis*, there is experimental evidence that the sensitivity to H<sub>2</sub>O<sub>2</sub> could be

regulated by the catalytic activity of the endogenous NUDT9H domain of NvTRPM2 (Kühn et al., 2016, 2019). In addition, our current study revealed significant expression of an orthologue of the human ADPRase NUDT9 in *N. vectensis*. Thus, the oxidative stress-induced accumulation of cytosolic ADPR as crucial trigger of NvTRPM2 activation might be suppressed by two independent ADPRases. This scenario could result in an increased threshold for the H<sub>2</sub>O<sub>2</sub>-dependent activation of NvTRPM2 *in vivo* and may be subject to a special, currently unknown regulatory mechanism.

In light of our finding that NvTRPM2 and NvNUDT9 are expressed in *N. vectensis*, it can be assumed that in this species ADP-ribose also plays an important role as an intracellular signalling molecule. Further studies will be necessary to compare the physiological relevance of ADPR in *N. vectensis* and other sea anemones with its pivotal role in mammals. The development of NUDT9-based ADPR-FRET sensors would represent a promising tool that may help with the analysis of cellular ADPR signalling processes in the future (Gattkowski et al., 2021).

Acute environmental stress, e.g. induced by shifts of temperature, pH and osmolarity, can interfere with the cellular redox balance, leading to the increased production of reactive oxygen species (Tomanek, 2015). However, the organism has the ability to adjust the production of antioxidant enzymes in response to acute fluctuations of local temperature. This is not only the case for marine invertebrates (Handy et al., 2009) but also generally occurs in all eukaryotic cells (González Durán et al., 2019). In addition, the mammalian TRPM2 channel has been described as sensitive both to oxidative stress and higher temperatures, whereby oxidative stress sensitizes TRPM2 to heat (Kashio et al., 2012; Kashio and Tominaga, 2017).

Therefore, regarding the effects of high temperature on the phenotype of wild-type and NvTRPM2<sup>1016Stop</sup> *N. vectensis*, similar results to those obtained by oxidative stress treatment were expected. Instead, our experimental findings revealed that NvTRPM2 attenuates tissue damage induced by high-temperature treatment, and thus exerts a protective function in *N. vectensis*. At first glance, this result seems difficult to reconcile with previous findings, in particular the stimulating effects of H<sub>2</sub>O<sub>2</sub> and higher temperatures on mammalian TRPM2 channels. However, it must be taken into

account that the activation mechanism of NvTRPM2 in *N. vectensis* is remarkably different from the mammalian orthologues. As mentioned above, the sensitivity of NvTRPM2 to H<sub>2</sub>O<sub>2</sub> strongly depends on the enzymatic activity of the endogenous NUDT9H domain, which is catalytically inactive in HsTRPM2 (Kühn et al., 2016, 2019; Iordanov et al., 2016, 2019). Furthermore, the temperature sensitivity of NvTRPM2 has not yet been investigated, and therefore it cannot be excluded that high temperatures do not directly affect NvTRPM2. It is conceivable that higher temperatures to a certain degree stimulate not only antioxidant enzymes (González Durán et al., 2019) but also ADPRases such as NUDT9 or the NUDT9H domain of NvTRPM2, leading to the degradation of the principal channel agonist ADPR. As a result, higher temperatures would attenuate rather than stimulate channel function of NvTRPM2. Nevertheless, all these considerations cannot explain our experimental findings, where in *N. vectensis*, loss of NvTRPM2 function aggravates tissue damage after exposure to high temperature.

Possibly, in *N. vectensis*, NvTRPM2 plays an entirely different physiological role in response to higher temperatures. Besides its well-established function as a mediator of oxidative stress-induced apoptosis in mammals, there is also experimental evidence from TRPM2 knockout mice that TRPM2 can protect cardiac myocytes from ischaemic injury by preventing mitochondrial dysfunction and increased ROS levels (Miller et al., 2014). In further studies, genetic deletion of TRPM2 in mice was also shown to be neuroprotective in a developmental model of hypoxic–ischaemic brain damage (Huang et al., 2017) or to reduce susceptibility to pneumoseptic infection by *Klebsiella pneumoniae* corresponding with decreased bacterial burden and attenuated tissue pathology (Tripathi et al., 2018). All these physiological processes are linked to specific regulation mechanisms that do not necessarily run via the classic ADPR pathway. However, a connection between the described protective role of TRPM2 and functional effects of higher temperature has not yet been investigated. At least in the case of infectious processes and the corresponding immune responses, a critical role of elevated temperatures in context with human TRPM2 is plausible (e.g. Knowles et al., 2013; Tan and McNaughton, 2018). However, the underlying mechanisms are not yet fully understood. Whether such processes in a rudimentary form also occur in marine invertebrates such as *N. vectensis* is of course completely open.

In conclusion, our experimental findings deliver first insights into the physiological role of TRPM2 in a basal metazoan and may open the door for detailed molecular studies on the stress response of *N. vectensis*. Further efforts are needed to examine thermoregulation of NvTRPM2 and to pinpoint the physiological role of ADPR in sea anemones. In this context, *N. vectensis* could represent a valuable model system to characterize the physiological spectrum of TRPM2 function.

#### Acknowledgements

We thank Marina Wolf for expert technical assistance.

#### Competing interests

The authors declare no competing or financial interests.

#### Author contributions

Conceptualization: F.R., F.J.P.K.; Methodology: W.E., J.M.G., F.R., F.J.P.K.; Validation: W.E., J.M.G., F.R., F.J.P.K.; Formal analysis: W.E., F.J.P.K.; Investigation: W.E., F.J.P.K.; Resources: F.R., F.J.P.K.; Data curation: W.E., F.J.P.K.; Writing - original draft: W.E., F.J.P.K.; Writing - review & editing: W.E., J.M.G., F.R., F.J.P.K.; Visualization: W.E., F.J.P.K.; Supervision: F.J.P.K.; Project administration: F.J.P.K.; Funding acquisition: F.J.P.K.

#### Funding

The study was supported by the Deutsche Forschungsgemeinschaft (DFG, grant KU 2271/4-3 to F.J.P.K.).

#### References

- Abele-Oeschger, D., Tüg, H. and Röttgers, R. (1997). Dynamics of UV-driven hydrogen peroxide formation on an intertidal sandflat. *Am. Soc. Limnol. Oceanography* **12**, 1406–1415. doi:10.4319/lo.1997.42.6.1406
- Bari, M. R., Akbar, S., Eweida, M., Kühn, F. J. P., Gustafsson, A. J., Lückhoff, A. and Islam, M. S. (2009). H<sub>2</sub>O<sub>2</sub>-induced Ca<sup>2+</sup> influx and its inhibition by N-(p-aminocinnamoyl) anthranilic acid in the beta-cells: involvement of TRPM2 channels. *J. Cell. Mol. Med.* **13**, 3260–3267. doi:10.1111/j.1582-4934.2009.00737.x
- Buelow, B., Song, Y. and Scharenberg, A. M. (2008). The Poly(ADP-ribose) polymerase PARP-1 is required for oxidative stress-induced TRPM2 activation in lymphocytes. *J. Biol. Chem.* **283**, 24571–24583. doi:10.1074/jbc.M802673200
- Darling, J. A., Reitzel, A. R., Burton, P. M., Mazza, M. E., Ryan, J. F., Sullivan, J. C. and Finnerty, J. R. (2005). Rising starlet: the starlet sea anemone, *Nematostella vectensis*. *BioEssays* **27**, 211–221. doi:10.1002/bies.20181
- Dias, M., Ferreira, A., Gouveia, R., Madeira, C., Jogee, N., Cabral, H., Diniz, M. and Vinagre, C. (2019). Long-term exposure to increasing temperatures on scleractinian coral fragments reveals oxidative stress. *Mar. Environ. Res.* **150**, 104758. doi:10.1016/j.marenvres.2019.104758
- Downs, C. A., Fauth, J. E., Halas, J. C., Dustan, P., Bemiss, J. and Woodley, C. M. (2002). Oxidative stress and seasonal coral bleaching. *Free Radic. Biol. Med.* **33**, 533–543. doi:10.1016/S0891-5849(02)00907-3
- Elran, R., Raam, M., Kraus, R., Brekhan, V., Sher, N., Plaschkes, I., Chalifa-Caspi, V. and Lotan, T. (2014). Early and late response of *Nematostella vectensis* transcriptome to heavy metals. *Mol. Ecol.* **23**, 4722–4736. doi:10.1111/mec.12891
- Fonfria, E., Marshall, I. C. B., Benham, C. D., Boyfield, I., Brown, J. D., Hill, K., Hughes, J. P., Skaper, S. D. and McNulty, S. (2004). TRPM2 channel opening in response to oxidative stress is dependent on activation of poly(ADP-ribose) polymerase. *Br. J. Pharmacol.* **143**, 186–192. doi:10.1038/sj.bjp.0705914
- Fonfria, E., Marshall, I. C. B., Boyfield, I., Skaper, S. D., Hughes, J. P., Owen, D. E., Zhang, W., Miller, B. A., Benham, C. D. and McNulty, S. (2005). Amyloid beta-peptide(1–42) and hydrogen peroxide-induced toxicity are mediated by TRPM2 in rat primary striatal cultures. *J. Neurochem.* **95**, 715–723. doi:10.1111/j.1471-4159.2005.03396.x
- Friedman, L. E., Gilmore, T. D. and Finnerty, J. R. (2018). Intraspecific variation in oxidative stress tolerance in a model cnidarian: Differences in peroxide sensitivity between and within populations of *Nematostella vectensis*. *PLoS ONE* **13**, e0188265. doi:10.1371/journal.pone.0188265
- Gattkowski, E., Rutherford, T. J., Möckl, F., Bauche, A., Sander, S., Fliegert, R. and Tidow, H. (2021). Analysis of ligand-binding and resulting conformational changes in pyrophosphatase NUDT9. *FEBS J.* **288**, 6769–6782. doi:10.1111/febs.16097
- González Durán, E., Cuaya, M. P., Gutiérrez, M. V. and León, J. A. (2019). Effects of temperature and pH on the oxidative stress of benthic marine invertebrates. *Biol. Bull.* **45**, 610–616. doi:10.1134/S1062359018660019
- Hand, C. and Uhlinger, K. R. (1992). The Culture, Sexual and Asexual Reproduction, and Growth of the Sea Anemone *Nematostella vectensis*. *Biol. Bull.* **182**, 169–176. doi:10.2307/1542110
- Handy, D., Lubos, E., Yang, Y., Galbraith, J. D., Kelly, N., Zhang, Y.-Y., Leopold, J. A. and Loscalzo, J. (2009). Glutathione peroxidase-1 regulates mitochondrial function to modulate redox-dependent cellular response. *J. Biol. Chem.* **284**, 11913–11921. doi:10.1074/jbc.M900392200
- Hara, Y., Wakamori, M., Ishii, M., Maeno, E., Nishida, M., Yoshida, T., Yamada, H., Shimizu, S., Mori, E., Kudoh, J. et al. (2002). LTRPC2 Ca<sup>2+</sup>-Permeable Channel Activated by Changes in Redox Status Confers Susceptibility to Cell Death. *Mol. Cell* **9**, 163–173. doi:10.1016/S1097-2765(01)00438-5
- Harter, V. L., Matthews, R. A. (2005). Acute and chronic toxicity test methods for *Nematostella vectensis* Stephenson. *Bull. Environ. Contam. Toxicol.* **74**, 830–836. doi:10.1007/s00128-005-0656-5
- Hecquet, C. M., Zhang, M., Mittal, M., Vogel, S. M., Di, A., Gao, X., Bonini, M. G. and Malik, A. B. (2014). Cooperative interaction of trp melastatin channel transient receptor potential (TRPM2) with its splice variant TRPM2 short variant is essential for endothelial cell apoptosis. *Circ. Res.* **114**, 469–479. doi:10.1161/CIRCRESAHA.114.302414
- Huang, S., Turlova, E., Li, F., Bao, M., Szeto, V., Wong, R., Abussaud, A., Wang, H., Zhu, S., Gao, X. et al. (2017). Transient receptor potential melastatin 2 channels (TRPM2) mediate neonatal hypoxic-ischemic brain injury in mice. *Exp. Neurol.* **296**, 32–40. doi:10.1016/j.expneurol.2017.06.023
- Huang, Y., Winkler, P. A., Sun, W., Lü, W. and Du, J. (2018). Architecture of the TRPM2 channel and its activation mechanism by ADP-ribose and calcium. *Nature* **562**, 145–149. doi:10.1038/s41586-018-0558-4

- Huang, Y., Roth, B., Lü, W. and Du, J. (2019). Ligand recognition and gating mechanism through three ligand-binding sites of human TRPM2 channel. *eLife* **8**, e50175. doi:10.7554/eLife.50175.029
- Ikmi, A., Mckinney, S. A., Delventhal, K. M. and Gibson, M. C. (2014). TALEN and CRISPR/Cas9-mediated genome editing in the early-branching metazoan *Nematostella vectensis*. *Nat. Commun.* **5**, 5486. doi:10.1038/ncomms6486
- Ikmi, A., Steenbergen, P. J., Anzo, M., McMullen, M. R., Stokkermans, A., Ellington, L. R. and Gibson, M. C. (2020). Feeding-dependent tentacle development in the sea anemone *Nematostella vectensis*. *Nat. Commun.* **11**, 4399. doi:10.1038/s41467-020-18133-0
- Iordanov, I., Mihályi, C., Tóth, B. and Csanády, L. (2016). The proposed channel-enzyme transient receptor potential melastatin 2 does not possess ADP ribose hydrolase activity. *Elife* **5**, e17600. doi:10.7554/eLife.17600
- Iordanov, I., Tóth, B., Szollosi, A. and Csanády, L. (2019). Enzyme activity and selectivity filter stability of ancient TRPM2 channels were simultaneously lost in early vertebrates. *Elife* **8**, e44556. doi:10.7554/eLife.44556
- Jahnel, S., Walzl, M. and Technau, U. (2014). Development and epithelial organisation of muscle cells in the sea anemone *Nematostella vectensis*. *Front. Zool.* **11**, 44. doi:10.1186/1742-9994-11-44
- Kashio, M., Sokabe, T., Shintaku, K., Uematsu, T., Fukuta, N., Kobayashi, N., Mori, Y. and Tominaga, M. (2012). Redox signal-mediated sensitization of transient receptor potential melastatin 2 (TRPM2) to temperature affects macrophage functions. *Proc. Natl. Acad. Sci. USA* **109**, 6745-6750. doi:10.1073/pnas.1114193109
- Kashio, M. and Tominaga, M. (2017). The TRPM2 channel: a thermo-sensitive metabolic sensor. *Channels* **11**, 426-433. doi:10.1080/19336950.2017.1344801
- Knowles, H., Li, Y. and Perraud, A.-L. (2013). The TRPM2 ion channel, an oxidative stress and metabolic sensor regulating innate immunity and inflammation. *Immunol. Res.* **55**, 241-248. doi:10.1007/s12026-012-8373-8
- Kraus, Y. and Technau, U. (2006). Gastrulation in the sea anemone *Nematostella vectensis* occurs by invagination and immigration: an ultrastructural study. *Dev. Genes Evol.* **216**, 119-132. doi:10.1007/s00427-005-0038-3
- Kraus, Y., Aman, A., Technau, U. and Genikhovich, G. (2016). Pre-bilaterian origin of the blastoporal axial organizer. *Nat. Commun.* **7**, 11694. doi:10.1038/ncomms11694
- Kühn, F. J. P. (2020). Structure-function relationship of TRPM2: recent advances, contradictions, and open questions. *Int. J. Mol. Sci.* **21**, 6481.
- Kühn, F. J. P., Kuhn, C. and Lückhoff, A. (2015). Functional characterisation of a TRPM2 orthologue from the sea anemone *Nematostella vectensis* in human cells. *Sci. Rep.* **5**, 8032. doi:10.1038/srep08032
- Kühn, F. J. P., Kühn, C., Winking, M., Hoffmann, D. C. and Lückhoff, A. (2016). ADP-ribose activates the trpm2 channel from the sea anemone *Nematostella vectensis* independently of the NUDT9H domain. *PLoS ONE* **11**, e0158060.
- Kühn, F. J. P., Kuhn, C. and Lückhoff, A. (2017). Different principles of ADP-ribose-mediated activation and opposite roles of the NUDT9 homology domain in the TRPM2 orthologs of man and sea anemone. *Front. Physiol.* **8**, 879. doi:10.3389/fphys.2017.00879
- Kühn, F. J. P., Ehrlich, W., Barth, D., Kühn, C. and Lückhoff, A. (2019). Functional importance of NUDT9H domain and N-terminal ADPR-binding pocket in two species variants of vertebrate TRPM2 channels. *Sci. Rep.* **9**, 19224. doi:10.1038/s41598-019-55232-5
- Layden, M. J., Rentzsch, F. and Rottinger, E. (2016). The rise of the starlet sea anemone *Nematostella vectensis* as a model system to investigate development and regeneration. *Wiley Interdiscip. Rev. Dev. Biol.* **5**, 408-428. doi:10.1002/wdev.222
- Lim, J. B., Langford, T. F., Huang, B. K., Deen, W. M. and Sikes, H. D. (2016). A reaction-diffusion model of cytosolic hydrogen peroxide. *Free Radic. Biol. Med.* **90**, 85-90. doi:10.1016/j.freeradbiomed.2015.11.005
- Magie, C. R., Daly, M. and Martindale, M. Q. (2007). Gastrulation in the cnidarian *Nematostella vectensis* occurs via invagination not ingression. *Dev. Biol.* **305**, 483-497. doi:10.1016/j.ydbio.2007.02.044
- Malko, P. and Jiang, L. H. (2020). TRPM2 channel-mediated cell death: An important mechanism linking oxidative stress-inducing pathological factors to associated pathological conditions. *Redox Biol.* **37**, 101755. doi:10.1016/j.redox.2020.101755
- Miller, D. J., Hemmrich, G., Ball, E. E., Hayward, D. C., Khalturin, K., Funayama, N., Agata, K. and Bosch, T. C. G. (2007). The innate immune repertoire in Cnidaria: ancestral complexity and stochastic gene loss. *Genome Biol.* **8**, R59. doi:10.1186/gb-2007-8-4-r59
- Miller, B. A., Hoffman, N. E., Merali, S., Zhang, X.-Q., Wang, J. F., Rajan, S., Shanmughapriya, S., Gao, E., Barrero, C. A., Mallilankaraman, K. et al. (2014). TRPM2 channels protect against cardiac ischemia-reperfusion injury: role of mitochondria. *J. Biol. Chem.* **289**, 7615-7629. doi:10.1074/jbc.M113.533851
- Miller, B. A. and Cheung, J. Y. (2016). TRPM2 protects against tissue damage following oxidative stress and ischaemia-reperfusion. *J. Physiol.* **594**, 4181-4191. doi:10.1113/JP270934
- Pascal, J. M. and Ellenberger, T. (2015). The rise and fall of poly(ADP-ribose): An enzymatic perspective. *DNA Repair* **32**, 10-16. doi:10.1016/j.dnarep.2015.04.008
- Perraud, A. L., Fleig, A., Dunn, C. A., Bagley, L. A., Launay, P., Schmitz, C., Stokes, A. J., Zhu, Q., Bessman, M. J., Penner, R. et al. (2001). ADP-ribose gating of the calcium-permeable LTRPC2 channel revealed by Nudix motif homology. *Nature* **411**, 595-599. doi:10.1038/35079100
- Perraud, A. L., Shen, B., Dunn, C. A., Rippe, K., Smith, M. K., Bessman, M. J., Stoddard, B. L. and Scharenberg, A. M. (2003). NUDT9, a member of the Nudix hydrolase family, is an evolutionarily conserved mitochondrial ADP-ribose pyrophosphatase. *J. Biol. Chem.* **278**, 1794-1801. doi:10.1074/jbc.M205601200
- Perraud, A. L., Takanishi, C. L., Shen, B., Kang, S., Smith, M. K., Schmitz, C., Knowles, H. M., Ferraris, D., Li, W., Zhang, J. et al. (2005). Accumulation of free ADP-ribose from mitochondria mediates oxidative stress-induced gating of TRPM2 cation channels. *J. Biol. Chem.* **280**, 6138-6148. doi:10.1074/jbc.M411446200
- Putnam, N., Srivastava, M., Hellsten, U., Dirks, B., Chapman, J., Salamov, A., Terry, A., Shapiro, H., Lindquist, E., Kapitonov, V. V. et al. (2007). Sea anemone genome reveals ancestral eumetazoan gene repertoire and genomic organization. *Science* **317**, 86-94. doi:10.1126/science.1139158
- Reitzel, A. M., Sullivan, J. C., Traylor-Knowles, N. and Finnerty, J. R. (2008). Genomic survey of candidate stress-response genes in the estuarine anemone *Nematostella vectensis*. *Biol. Bull.* **214**, 233-254. doi:10.2307/25470666
- Reitzel, A., Chu, T., Edquist, S., Genovese, C., Church, C., Tarrant, A. M. and Finnerty, J. R. (2013). Physiological and developmental responses to temperature by the sea anemone *Nematostella vectensis*. *Mar. Ecol. Prog. Ser.* **484**, 115-130. doi:10.3354/meps10281
- Shearer, M., Suwailam, M. and Rowe, G. (1997). The anemone, *Nematostella vectensis*, in Britain: considerations for conservation management. *Aquat. Conserv.* **7**, 13-25. doi:10.1002/(SICI)1099-0755(199703)7:1<13::AID-AQC210>3.0.CO;2-Y
- Song, K., Wang, H., Kamm, G. B., Pohle, J., Reis, F. C., Heppenstall, P., Wende, H. and Siemens, J. (2016). The TRPM2 channel is a hypothalamic heat sensor that limits fever and can drive hypothermia. *Science* **353**, 1393-1398. doi:10.1126/science.aaf7537
- Stefanik, D. J., Friedman, L. E. and Finnerty, J. R. (2013). Collecting, rearing, spawning and inducing regeneration of the starlet sea anemone, *Nematostella vectensis*. *Nat. Protoc.* **8**, 916-923. doi:10.1038/nprot.2013.044
- Sullivan, J. C., J. F. Ryan, J. A. Watson, J. Webb, J. C. Mullikin, D. Rokhsar, J. R. and Finnerty, (2006). StellaBase: the *Nematostella vectensis* genomics database. *Nucleic Acids Res.* **34**, D495-D499. doi:10.1093/nar/gkj020
- Sun, L., Yau, H.-Y., Wong, W.-Y., Li, R. A., Huang, Y. and Yao, X. (2012). Role of TRPM2 in H<sub>2</sub>O<sub>2</sub>-induced cell apoptosis in endothelial cells. *PLoS ONE* **7**, e43186. doi:10.1371/journal.pone.0043186
- Tan, C. H. and McNaughton, P. A. (2016). The TRPM2 ion channel is required for sensitivity to warmth. *Nature* **536**, 460-463. doi:10.1038/nature19074
- Tan, C. H. and McNaughton, P. A. (2018). TRPM2 and warmth sensation. *Pflugers Arch.* **470**, 787-798. doi:10.1007/s00424-018-2139-7
- Tarrant, A. M., Reitzel, A. M., Kwok, C. K. and Jenny, M. J. (2014). Activation of the cnidarian oxidative stress response by ultraviolet radiation, polycyclic aromatic hydrocarbons and crude oil. *J. Exp. Biol.* **217**, 1444-1453. doi:10.1242/jeb.093690
- Technau, U., Rudd, S., Maxwell, P., Gordon, P. M. K., Saina, M., Grasso, L. C., Hayward, D. C., Sensen, C. W., Saint, R., Holstein, T. W. et al. (2005). Maintenance of ancestral complexity and non-metazoan genes in two basal cnidarians. *Genome Analysis* **21**, 633-639. doi:10.1016/j.tig.2005.09.007
- Tomanek, L. (2015). Proteomic responses to environmentally induced oxidative stress. *J. Exp. Biol.* **218**, 1867-1879. doi:10.1242/jeb.116475
- Tripathi, J. K., Sharma, A., Sukumaran, P., Sun, Y., Mishra, B. B., Singh, B. B. and Sharma, J. (2018). Oxidant sensor cation channel TRPM2 regulates neutrophil extracellular trap formation and protects against pneumoseptic bacterial infection. *FASEB J.* **32**, fj201800605. doi:10.1096/fj.201800605
- Uchida, K., Dezaki, K., Damdindorj, B., Inada, H., Shiuchi, T., Mori, Y., Yada, T., Minokoshi, Y. and Tominaga, M. (2011). Lack of TRPM2 impaired insulin secretion and glucose metabolisms in mice. *Diabetes* **60**, 119-126. doi:10.2337/db10-0276
- Vriens, J., Owsianik, G., Fisslthaler, B., Suzuki, M., Janssens, A., Voets, T., Morisseau, C., Hammock, B. D., Fleming, I., Busse, R. et al. (2005). Modulation of the Ca<sup>2+</sup> permeable cation channel TRPV4 by cytochrome P450 epoxygenases in vascular endothelium. *Circ. Res.* **97**, 908-915. doi:10.1161/01.RES.0000187474.47805.30
- Wehage, E., Eisfeld, J., Heiner, I., Jüngling, E., Zitt, C. and Lückhoff, A. (2002). Activation of the cation channel long transient receptor potential channel 2 (LTRPC2) by hydrogen peroxide. A splice variant reveals a mode of activation independent of ADP-ribose. *J. Biol. Chem.* **277**, 23150-23156. doi:10.1074/jbc.M112096200
- Winking, M., Hoffmann, D. C., Kühn, C., Hilgers, R.-D., Lückhoff, A. and Kühn, F. J. P. (2012). Importance of a conserved sequence motif in transmembrane segment S3 for the gating of human TRPM8 and TRPM2. *PLoS One* **7**, e49877. doi:10.1371/journal.pone.0049877

- Yamamoto, S., Shimizu, S., Kiyonaka, S., Takahashi, N., Wajima, T., Hara, Y., Negoro, T., Hiroi, T., Kiuchi, Y., Okada, T. et al.** (2008). TRPM2-mediated  $\text{Ca}^{2+}$  influx induces chemokine production in monocytes that aggravates inflammatory neutrophil infiltration. *Nat. Med.* **14**, 738-747. doi:10.1038/nm1758
- Zhang, W., Chu, X., Tong, Q., Cheung, J. Y., Conrad, K., Masker, K. and Miller, B. A.** (2003). A novel TRPM2 isoform inhibits calcium influx and susceptibility to cell death. *J. Biol. Chem.* **278**, 16222-16229. doi:10.1074/jbc.M300298200
- Zou, J., Ainscough, J. F., Yang, W., Sedo, A., Yu, S.-P., Mei, Z.-Z., Sivaprasadarao, A., Beech, D. J. and Jiang, L.-H.** (2013). A differential role of macrophage TRPM2 channels in  $\text{Ca}^{2+}$  signaling and cell death in early responses to  $\text{H}_2\text{O}_2$ . *Am. J. Physiol. Cell Physiol.* **305**, C61-C69. doi:10.1152/ajpcell.00390.2012

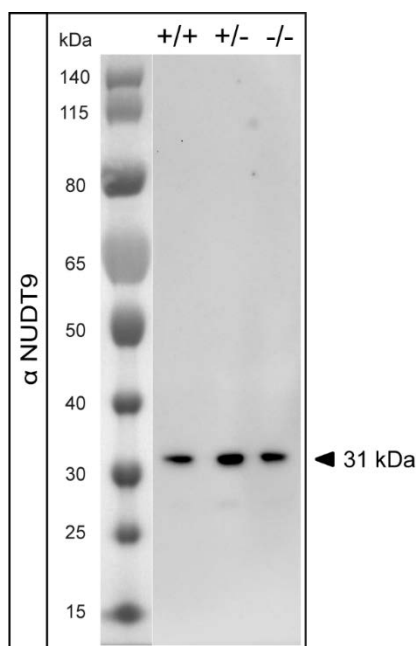


**Fig. S1.** An orthologue of the human NUDT9 enzyme is expressed in wildtype as well as heterozygous and homozygous  $NvTRPM2^{1016Stop}$  animals of *Nematostella*. The NUDT9 expression in total cell lysates was analysed with adult individuals of *Nematostella* using SDS-PAGE gel electrophoresis and Western blot analysis. Parts of the head and foot of wildtype (+/+), heterozygous (+/-) and homozygous (-/-)  $NvTRPM2^{1016Stop}$  animals were dissected and lysed. The same single protein band which corresponds to a protein mass of 31 kDa was detected using a commercially available anti-human NUDT9 antiserum in all three different genotypes examined. Three independent experiments gave similar results.

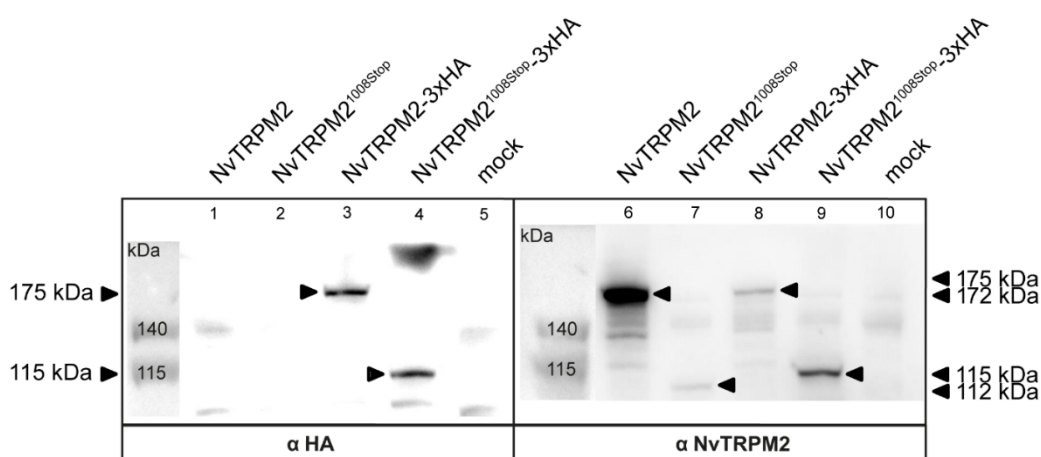


**Fig. S2.** Total expression of  $NvTRPM2$  and  $NvTRPM2^{1008Stop}$  channels in HEK-293 cells. Lysates of cells, heterologously expressing wild-type  $NvTRPM2$  or  $NvTRPM2^{1008Stop}$  either with or without 3x-HA tag, were analysed by SDS-PAGE gel electrophoresis and Western blot analysis. Mock-transfected cells were used as negative control. Screening with anti-HA-antiserum (left panel) revealed bands ( $NvTRPM2$ -3xHA: 175 kDa,  $NvTRPM2^{1008Stop}$ -3xHA: 115 kDa) only in cell lysates with 3xHA-tagged channel variants. Screening with anti- $NvTRPM2$ -antiserum (right panel) both revealed bands ( $NvTRPM2$ : 172 kDa,  $NvTRPM2^{1008Stop}$ : 112 kDa) in cell lysates with the untagged channel variants and bands ( $NvTRPM2$ -3xHA: 175 kDa,  $NvTRPM2^{1008Stop}$ -3xHA: 115 kDa) in cell lysates with 3xHA-tagged channel variants.

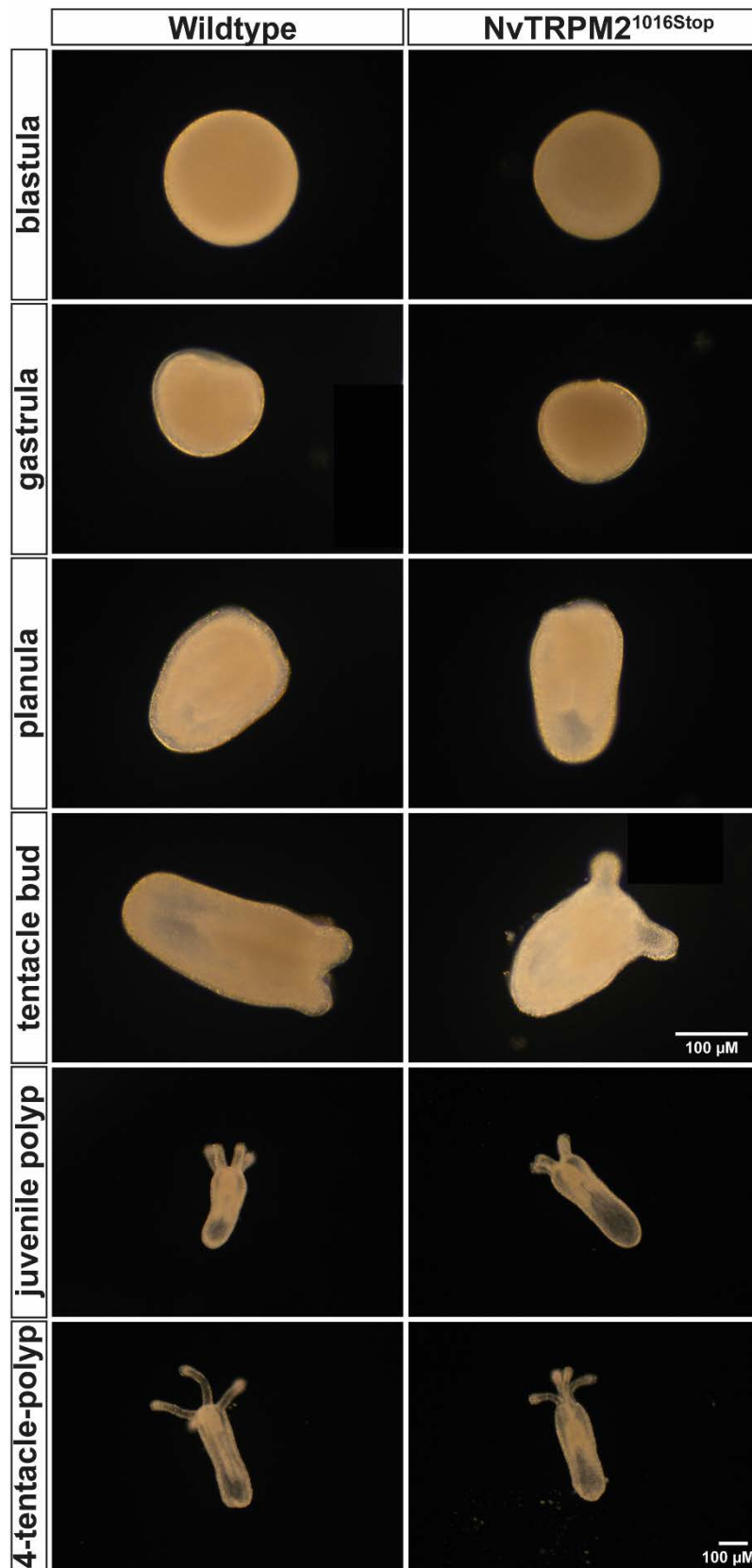


**Fig. S3. Comparison of the phenotypes of different developmental stages of wildtype and *NvTRPM2*<sup>1016Stop</sup> animals.** The physical appearance of representative larval stages of both genotypes are shown. No significant differences were found. The upper scale bar applies for the six upper bright-field images, the lower scale bar applies for the four lower bright-field images, both represent 100  $\mu$ m.